© 2022. Published by The Company of Biologists Ltd | Development (2022) 149, dev199931. doi:10.1242/dev.199931

RESEARCH ARTICLE

PAR3 restricts the expansion of neural precursor cells by regulating hedgehog signaling

Tomonori Hirose[1,2,*], Yoshinobu Sugitani[2,3], Hidetake Kurihara[4,5], Hiromi Kazama[1], Chiho Kusaka[1], Tetsuo Noda[2,6], Hidehisa Takahashi[1,*] and Shigeo Ohno[1,*]

ABSTRACT

During brain development, neural precursor cells (NPCs) expand initially, and then switch to generating stage-specific neurons while maintaining self-renewal ability. Because the NPC pool at the onset of neurogenesis crucially affects the final number of each type of neuron, tight regulation is necessary for the transitional timing from the expansion to the neurogenic phase in these cells. However, the molecular mechanisms underlying this transition are poorly understood. Here, we report that the telencephalon-specific loss of PAR3 before the start of neurogenesis leads to increased NPC proliferation at the expense of neurogenesis, resulting in disorganized tissue architecture. These NPCs demonstrate hyperactivation of hedgehog signaling in a smoothened-dependent manner, as well as defects in primary cilia. Furthermore, loss of PAR3 enhanced ligand-independent ciliary accumulation of smoothened and an inhibitor of smoothened ameliorated the hyperproliferation of NPCs in the telencephalon. Thus, these findings support the idea that PAR3 has a crucial role in the transition of NPCs from the expansion phase to the neurogenic phase by restricting hedgehog signaling through the establishment of ciliary integrity.

KEY WORDS: PAR3 (PARD3), Neurogenesis, Telencephalon, Hedgehog signaling, Primary cilia, Mouse

INTRODUCTION

Differentiated neurons do not proliferate, and therefore it is necessary to generate and maintain a large reserve of neural precursor cells (NPCs) in order to generate the vast number of neurons during brain development (Lui et al., 2011; Rakic, 1995). Indeed, during the initial expansion phase, NPCs exclusively undergo proliferative symmetric divisions to generate a sufficiently large pool of themselves. During the following neurogenic phase, NPCs go through irreversible differentiative asymmetric divisions to produce self-renewing NPCs as well as differentiated intermediate progenitors or specific subtypes of neurons in a developmental stage-specific manner (Miyata et al., 2010; Taverna et al., 2014). During development of the mouse telencephalon, the expansion and neurogenic phases correspond to approximately embryonic days (E) 8.5-E10.5 and E10.5-E17.5, respectively (Takahashi et al., 1999). Thus, to generate the appropriate number and diversity of neurons, it is essential to control the timing of the transition from the expansion to neurogenic phase of NPC division at approximately E10.5. In mouse NPCs, several cellular characteristics differ between these phases, including the location of mitosis within the tissue (Haubensak et al., 2004; Miyata et al., 2004), the proliferative capacity (Calegari, 2005) and the cleavage plane orientation to the ventricular surface (Postiglione et al., 2011; Shitamukai et al., 2011). Therefore, these complex cellular changes need to be carefully orchestrated during the transition from the expansion to the neurogenic phase (Miyata et al., 2010; Taverna et al., 2014). This phase transition has been demonstrated to depend on Notch (Hatakeyama et al., 2004) and FGF (Sahara and O'Leary, 2009) signaling, as well as all-trans retinoic acid secreted from the meninges (Siegenthaler et al., 2009). However, our understanding of the underlying mechanisms is still limited.

NPCs in the developing mouse telencephalon exhibit apicobasal cell polarity and cell division characteristics that differ according to their self-renewal capacity (Haubensak et al., 2004; Miyata et al., 2004; Taverna et al., 2014). Undifferentiated NPCs have a highly polarized and elongated morphology, and face the basement membrane and the ventricle, where they repeat self-renewal divisions, and their nuclei are tightly packed to form the ventricular zone (Taverna et al., 2014). Another type of self-renewing NPC, outer subventricular zone (OSVZ) progenitors, which possess only the basal processes without the apical domains required to detach from the ventricle, was identified in primates and other mammals (Fietz et al., 2010; Hansen et al., 2010). Moreover, intermediate progenitors committed to the neural lineage lost their apical domains and divided away from the ventricle to produce pairs of neurons without self-renewal ability (Miyata et al., 2004; Taverna et al., 2014). Given the importance of the balance between these NPC subtypes, various proteins regulating apicobasal cell polarity have been studied in the context of neurogenesis, including atypical protein kinase Cλ (aPKCλ) (Imai et al., 2006), Cdc42 (Cappello et al., 2006), Llgl1 (Jossin et al., 2017) and PAR3. Among the evolutionarily conserved polarity regulators, PAR3 appears to have dual roles in the proliferation and differentiation of mouse NPCs that differ in a developmental stage-specific manner. During the early neurogenic phase, PAR3 is required for neurogenic divisions by limiting Hippo signaling for self-renewal proliferation in the mouse dorsal telencephalon (Liu et al., 2018), whereas it inhibits neuronal differentiation by promoting proliferative divisions via Notch signaling in the mid-neurogenic phase (Bultje et al., 2009; Costa et al., 2008). Although such differences are crucial for the transition from the expansion to the neurogenic phase during neurogenesis, the functions of PAR3 during this phase transition have not been reported to date.

[1]Department of Molecular Biology, Yokohama City University School of Medicine, Yokohama 236-0004, Japan. [2]Department of Cell Biology, Cancer Institute, Japanese Foundation for Cancer Research, Tokyo 135-8550, Japan. [3]Department of Pathology and Oncology, Juntendo University School of Medicine, Tokyo 113-8421, Japan. [4]Department of Anatomy and Life Structure, Juntendo University Graduate School of Medicine, Tokyo 113-8421, Japan. [5]Department of Physical Therapy, Faculty of Health Science, Aino University, Osaka 567-0012, Japan. [6]Director's Room, Cancer Institute, Japanese Foundation for Cancer Research, Tokyo 135-8550, Japan.

*Authors for correspondence (thirose@yokohama-cu.ac.jp; hide0213@yokohama-cu.ac.jp; ohnos@yokohama-cu.ac.jp)

T.H., 0000-0003-2428-0919; H.Kurihara, 0000-0001-8670-0224; H.T., 0000-0001-7181-9863; S.O., 0000-0002-1294-5269

Handling Editor: James Briscoe
Received 27 June 2021; Accepted 3 October 2022

Development (2022) 149, dev199931. doi:10.1242/dev.199931

The hedgehog (Hh) family of ligands, including sonic hedgehog (Shh), function as mitogens by binding to the 12-pass transmembrane receptor patched 1 (Ptch1), which is a negative regulator for the seven-pass transmembrane protein smoothened (Smo). Upon ligand binding, Ptch1 releases Smo, which then mediates the activation of Gli transcription factors, resulting in the induction of target genes (Briscoe and Thérond, 2013). In vertebrates, the primary cilia provide an environment that is essential for Hh signaling (Briscoe and Thérond, 2013; Goetz and Anderson, 2010). Indeed, the ciliary localization of Ptch1, Smo and Gli proteins is key for the regulation of Hh signaling (Corbit et al., 2005; Haycraft et al., 2005; Rohatgi et al., 2007). Moreover, the phenotypes observed in many human congenital disorders and mutant animals with ciliary defects were linked to compromised Hh signaling, ranging from blockade to inappropriate activation (Bangs and Anderson, 2017; Goetz and Anderson, 2010). During mouse brain development, Hh signaling is required for ventral telencephalic patterning in the initial phase (Fuccillo et al., 2004; Rallu et al., 2002) and maintenance of NPC proliferation during the neurogenic phase (Komada et al., 2008; Palma and Ruiz i Altaba, 2004). In addition to these stage-specific functional differences, a single-cell gene profiling study revealed that Hh signaling activity was significantly higher in undifferentiated NPCs than in committed neural progenitors (Kawaguchi et al., 2008). Furthermore, hyperactivation of Hh signaling induced robust NPC expansion and neocortical growth (Matsumoto et al., 2020; Wang et al., 2016). Together, these observations suggest that tight temporal regulation of Hh signaling is essential for telencephalic development (Sousa and Fishell, 2010; Yabut and Pleasure, 2018). However, little is known about the mechanisms involved in this regulation.

Here, we show that mouse PAR3 is required for the appropriate transition of NPCs from the expansion to the neurogenic phase in the telencephalon by temporally regulating NPC proliferation. Loss of PAR3 results in hyperproliferation of NPCs and hyperactivation of Hh signaling with inappropriate accumulation of Smo in defective primary cilia. Together with the effects of the inhibition of Smo, our observations support the idea that PAR3 restricts NPC expansion through the establishment of ciliary integrity in the apical domain.

RESULTS

Foxg1-Cre-mediated selective deletion of PAR3 in the telencephalon

To study the role of PAR3 during the early neurogenic phase in the telencephalon, we immunolabeled a neuron-specific βIII tubulin, TuJ1 (Tubb3), in PAR3-deficient ($Par3^{\Delta E3/\Delta E3}$) and control forebrains at E11.5 (Fig. S1A,B). Although we found abnormal neural layer development in the $Par3^{\Delta E3/\Delta E3}$ telencephalon and diencephalon (Fig. S1B), mid-gestational embryonic lethality caused by defective cardiac development hampered further analysis (Hirose et al., 2006). To circumvent the embryonic lethality, we established a mouse line harboring a conditional *Par3* mutant allele ($Par3^{floxE3}$; Fig. 1A-C) and employed a *Foxg1-Cre* knock-in mouse line [$Foxg1^{tm1(cre)Skm}$] to induce selective deletion of the *Par3* gene in the emerging telencephalic region starting at approximately E8.0-E8.5 (Fig. S1C), before the expansion phase (Hébert and McConnell, 2000). Because this *Foxg1-Cre* mouse line exhibits size reduction of the dentate gyrus caused by haploinsufficiency of the *Foxg1* gene (Shen et al., 2006), we compared the $Foxg1^{+/Cre}$;$Par3^{floxE3/\Delta E3}$ conditional knockout (referred to as *Par3* cKO hereafter) embryos with $Foxg1^{+/Cre}$;$Par3^{floxE3/+}$ embryos, as controls, unless otherwise indicated. We examined PAR3 expression by immunofluorescence at E9.5. As previously observed (Manabe et al., 2002), PAR3 was clearly localized to the apical cell–cell junctions of neuroepithelial cells in the control telencephalon and spinal cord (Fig. 1E,F). We confirmed these PAR3 signals were markedly reduced in the *Par3* cKO telencephalon, but not in the spinal cord, with preservation of ZO-1 (Tjp1) at the apical cell–cell junctions (Fig. 1G,H). Next, we examined PAR3 by immunoblotting proteins extracted from the telencephalon at E10.5. The long isoform of PAR3 protein was detected in control samples but was consistently decreased in all *Par3* cKO samples (Fig. 1D; $*P=0.015$ determined by two-tailed Welch's *t*-test; $n=3$). Furthermore, we obtained *Par3* cKO embryos almost at the expected Mendelian ratio throughout embryonic stages E9.5 to E18.5 (26.3%; $n=378/1436$). These data indicate that our *Par3* cKO mouse line exhibits selective depletion of PAR3 in the telencephalon prior to the onset of the neurogenic phase without embryonic lethality.

Selective loss of PAR3 in the telencephalon enhances the proliferation of NPCs and results in ectopic neurogenesis

Although the gross appearance of the *Par3* cKO telencephalon at E10.5 was indistinguishable from controls (Fig. S2A,B), histological analysis revealed an irregular pial surface and thicker telencephalic tissues (Fig. 2B). Alongside this abnormal tissue architecture, the *Par3* cKO telencephalon had densely packed nuclei around the ventricle, indicating the formation of the ventricular zone. To assess the proliferation and differentiation of embryonic NPCs, the embryonic telencephalon was immunolabeled for pulse-labeled 5-bromo-2′-deoxyuridine (BrdU) or TuJ1. In the control telencephalon, as previously reported, many mitotic cells were aligned at the ventricular surface, with BrdU-positive NPC nuclei forming a zone on the outer side of the ventricular zone, and TuJ1-positive neural cells forming the outermost layer in the telencephalon (Fig. 2A). However, the *Par3* cKO telencephalon appeared to contain more BrdU-positive nuclei, which neither formed a clear zone nor were distributed within the ventricular zone (Fig. 2B). Moreover, TuJ1-positive neurons formed an irregular layer on the outermost region and were also ectopically distributed to the inner region (Fig. 2B, arrowheads). We also found many mitotic cells ectopically localized between these TuJ1-positive outermost and inner regions. These data indicate dysregulated proliferation and differentiation of *Par3* cKO NPCs before and during the initiation of the neurogenic phase.

To investigate the consequence of these defects, we examined embryos at later stages: E11.5 and E18.5. At E11.5, the control neuronal layer continued to thicken normally during development, and more BrdU-positive nuclei were aligned to the outer side of the ventricular zone (Fig. 2D). In contrast, the *Par3* cKO neuronal layer developed an aberrant architecture, including many ectopic BrdU-positive nuclei and mitotic NPCs (Fig. 2E). Moreover, a substantial number of BrdU-positive nuclei formed a zone in the outer side of the ventricular zone in a manner similar to controls. These telencephalic phenotypes are highly reminiscent of those observed in $Par3^{\Delta E3/\Delta E3}$ brains (Fig. S1B); however, no apparent defects were found in the *Par3* cKO diencephalon (Fig. 2C,E). Although the size of the *Par3* cKO telencephalon at E18.5 was comparable to controls, they displayed an irregular translucency and smaller olfactory bulbs (Fig. 2F). Indeed, *Par3* cKO telencephalic structures were severely perturbed, with overall hypertrophy, resulting in smaller ventricles, disturbed cortical layers and the formation of neural rosettes (Fig. 2G, right). These data consistently demonstrated that *Par3* cKO NPCs had high proliferative activity, with preservation of their differentiation potential into neurons to a certain extent. There were

Development (2022) 149, dev199931. doi:10.1242/dev.199931

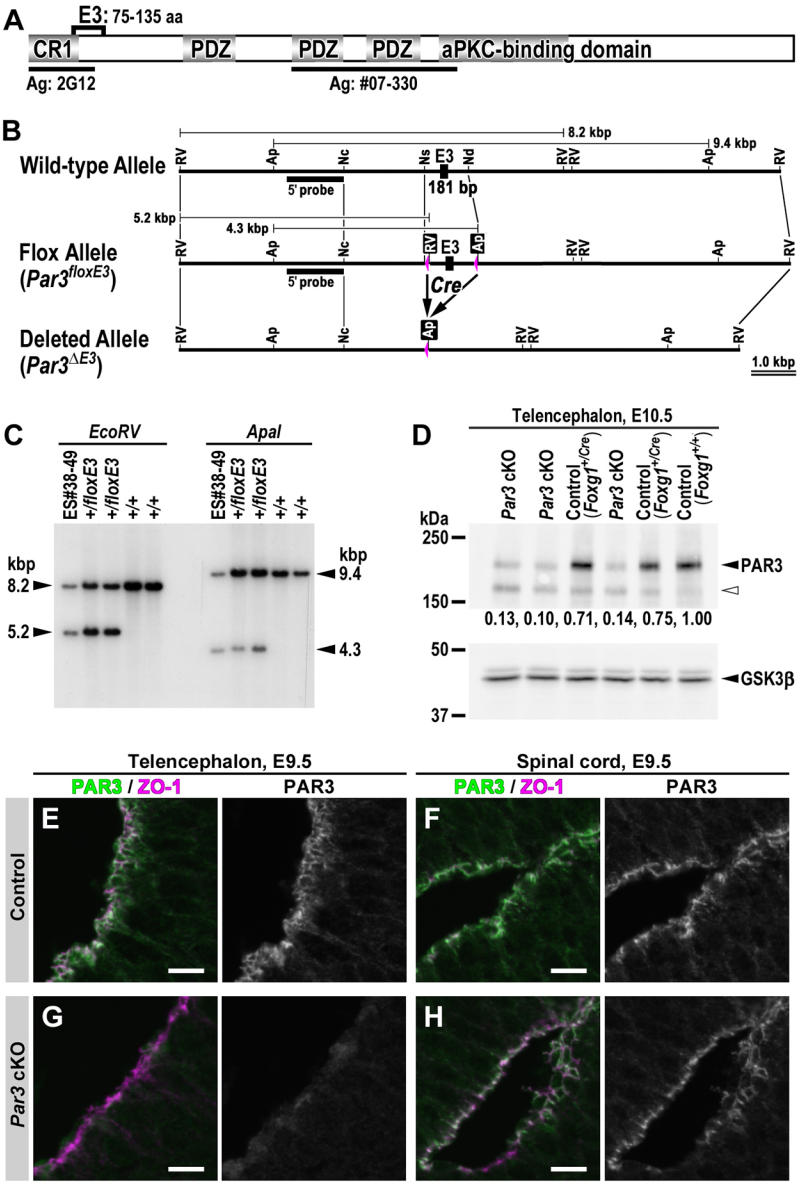

Fig. 1. *Foxg1-Cre*-mediated conditional disruption of the *Par3* gene. (A) Schematic structure of the PAR3 protein with the conserved oligomerization (CR1), three PDZ, and aPKC-binding domains. The third coding exon (E3; 181 bp) encodes amino acids 75-135. Black bars indicate the antigenic regions for anti-PAR3 mAb (2G12) and pAb (#07-330). (B) Restriction maps of wild-type, flox (*Par3*^{floxE3}) and deleted (*Par3*$^{\Delta E3}$) mouse *Par3* alleles. The loxP sequences are shown as magenta triangles. Black bars indicate the position of the 5′ probe for the Southern blot analysis shown in C. Ap, ApaI; Nc, NcoI; Nd, NdeI; Ns, NsiI; RV, EcoRV. (C) Southern blot analysis of EcoRV- or ApaI-digested genomic DNA from the original ESC clone and four F1 pups derived from the chimeric mouse. The genomic region corresponding to each band is indicated in B. (D) Immunoblotting for PAR3 using anti-PAR3 pAb (07-330) in total protein extracts from dissected telencephalons at E10.5. The values below the bands show relative intensities of PAR3 normalized to GSK3β. The genotypes of control embryos are *Foxg1*$^{+/Cre}$;*Par3*$^{floxE3/+}$ or *Foxg1*$^{+/+}$;*Par3*$^{floxE3/+}$. The white arrowhead indicates extra bands exclusively detected in the samples with, but not without, the recombined *Par3*$^{\Delta E3}$ allele generated by *Foxg1-Cre*. The deletion of the third coding exon may induce a cryptic *Par3* transcript. (E-H) Immunofluorescence of PAR3, using anti-PAR3 mAb (2G12), and ZO-1 in the telencephalon and spinal cord of control and *Par3* cKO littermates at E9.5 (22 somites each). Scale bars: 10 µm.

no viable *Par3* cKO newborn pups (0/19 *Par3* cKO pups from 13 litters), or failures to resuscitate after cesarean section at E18.5 (successful resuscitation in two litters examined: *Par3* cKO pups, 0/3; other littermates, 12/13), indicating neonatal lethality in *Par3* cKO pups. Importantly, conditional deletion of PAR3 with the *Nestin-Cre* transgene (*NesCre*$^{Tg+}$;*Par3*$^{floxE3/\Delta E3}$) exhibited much milder phenotypes (Fig. 2H,I) than those in the *Par3* cKO telencephalon (Fig. 2B,E). The observation that the *Nestin-Cre* transgene induced NPC-selective recombination in the early neurogenic phase around E11.5, about 3 days later than that of *Foxg1-Cre* (Fig. S1C,D) (Imai et al., 2006), indicates that PAR3 has a crucial role in NPCs before the neurogenic phase. Taken together, our observations indicate that PAR3 is required for the appropriate regulation of NPC proliferation within a narrow window of development to establish normal telencephalic tissue architecture.

Impaired morphology and interkinetic nuclear migration of *Par3* cKO NPCs

The histological disorganization of the *Par3* cKO telencephalon prompted us to assess the radial alignment and bipolar morphology of the NPCs. Immunofluorescence of the phosphorylated forms of vimentin and nestin, or pericentrin can mark radial fibers and the orientation of apical domains, respectively (Hansen et al., 2010; Imai et al., 2006). In control telencephalons at E10.5 and E11.5, we consistently confirmed that elongated NPCs were radially aligned with apical domains facing the ventricle and dividing mainly at the ventricular surface (Fig. 3A-C; Fig. S2C). These observations are consistent with previous reports of interkinetic nuclear migration (INM), i.e. the nuclei of NPCs translocate toward the ventricular surface along the radially aligned cell bodies during mitosis, and the daughter nuclei migrate away after mitosis (Noctor et al., 2001; Sauer, 1935). In the *Par3* cKO telencephalon, many NPCs in the outer region displayed a disturbed radial orientation with tangled processes (Fig. 3D-H; Fig. S2D). Immunofluorescence of pericentrin and β-catenin revealed many ectopic divisions of NPCs with rearranged cell–cell junctions away from the ventricular surface (Fig. 3E,G, arrowheads). Of note, *Par3* cKO NPCs facing the ventricular surface had no obvious perturbations in apical junctions at E10.5 (Fig. S2F), but junctional proteins were diminished in the lateral

Development (2022) 149, dev199931. doi:10.1242/dev.199931

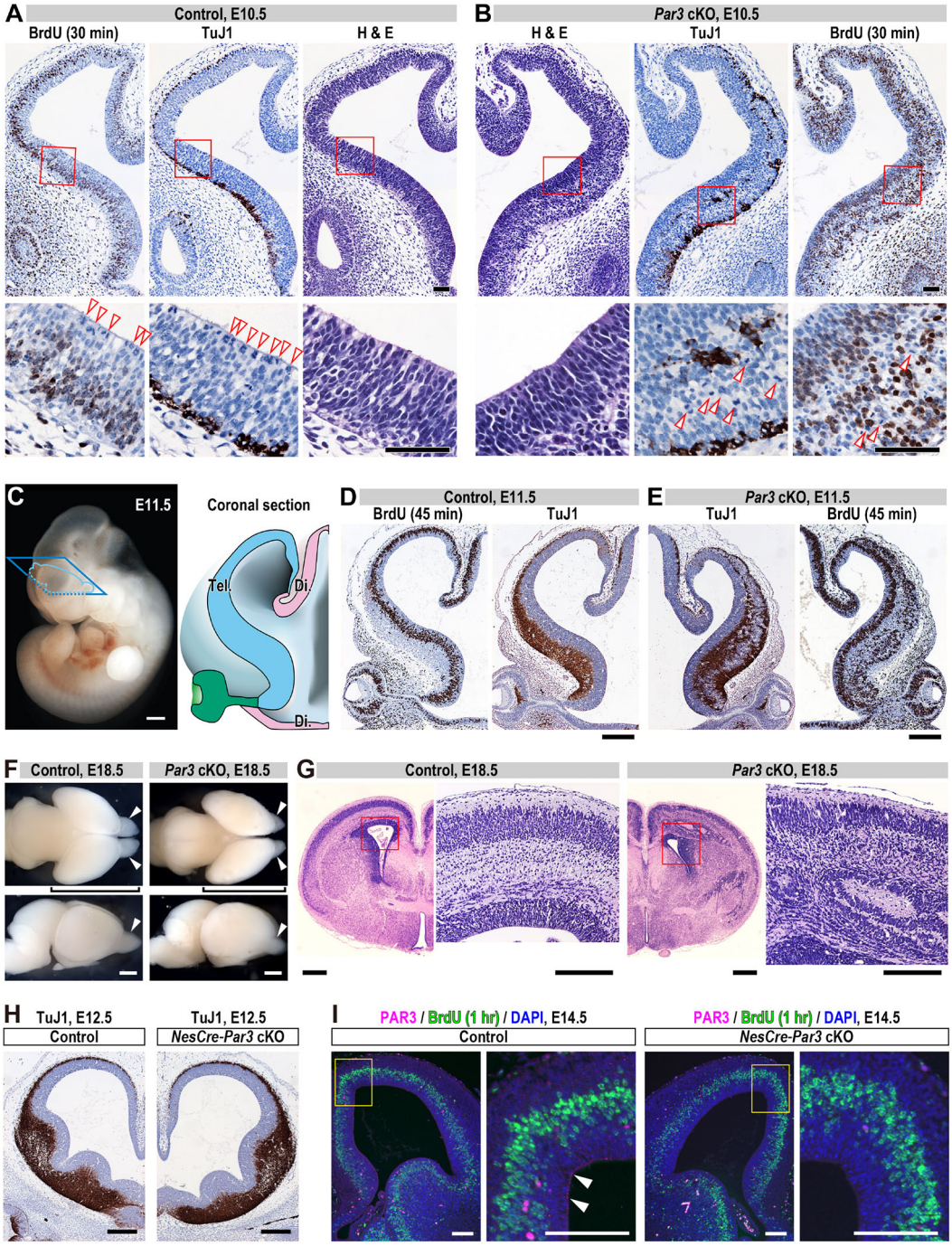

Fig. 2. Loss of PAR3 in the telencephalon results in hyperproliferation of NPCs and hypertrophy of the telencephalon. (A-E) Immunohistochemistry of pulse-labeled BrdU and TuJ1, and Hematoxylin and Eosin (H&E) staining in coronal sections of control and *Par3* cKO telencephalons at E10.5 (A,B) or E11.5 (D,E). Arrowheads indicate mitotic figures. Schematic in C shows a coronal section of the forebrain including the telencephalon (Tel., blue), diencephalon (Di., pink) and optic cup (green) at E11.5. (F) Whole-mount brains of control and *Par3* cKO littermates at E18.5. Brackets and arrowheads indicate telencephalons and olfactory bulbs, respectively. (G) H&E staining of coronal sections from control and *Par3* cKO littermate telencephalons at E18.5. (H,I) Immunohistochemistry of TuJ1, immunofluorescence of PAR3 and pulse-labeled BrdU, and DAPI staining in the telencephalons of control and *Nestin-Cre*-mediated *Par3* mutant telencephalons at E12.5 (H) or E14.5 (I). Arrowheads indicate PAR3 localized at cell–cell junctions of the ventricular surface. Red and yellow boxes correspond to the regions magnified alongside. To cover wide areas, low (A,B) and high (G) power images were prepared by merging two photos each. Scale bars: 50 µm (A,B); 0.5 mm (C); 200 µm (D,E,G-I); 1 mm (F).

ganglionic eminence by E15.5 (Fig. S2H). Instead, some NPCs in the outer region lost apical domains but extended basal processes to the pial surface at E11.5 (Fig. 3H). Including ectopic NPCs, *Par3* cKO NPCs showed intense nuclear accumulation of Sox2 and cleaved intracellular domain of Notch1, similar to control telencephalon (Fig. 3I,J). These observations indicate that, despite the abnormal morphology and distribution, ectopic NPCs had preserved self-renewal activity at a level similar to that of the other and control NPCs (Hansen et al., 2010; Mizutani et al., 2007).

Development (2022) 149, dev199931. doi:10.1242/dev.199931

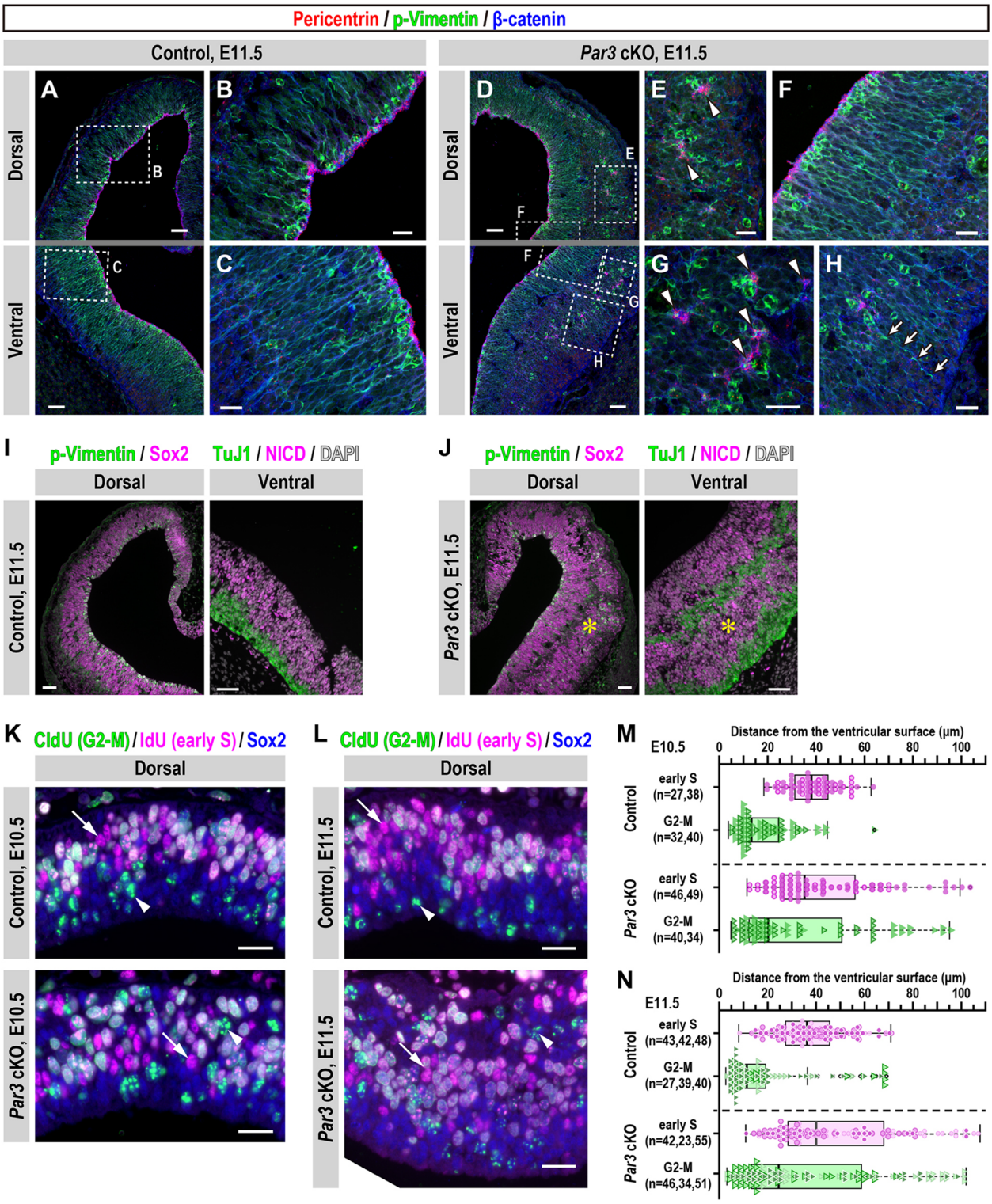

Fig. 3. Loss of PAR3 in the telencephalon perturbs tissue architecture and interkinetic nuclear migration. (A-H) Representative immunofluorescence for pericentrin, vimentin phosphorylated on Ser55 (p-vimentin) and β-catenin in coronal sections of control and *Par3* cKO telencephalons at E11.5. Dashed rectangles correspond to the magnified regions alongside. Arrowheads indicate ectopic clustering of pericentrin. Arrows indicate a cell process extending from a dividing NPC. (I,J) Representative immunofluorescence of p-vimentin and Sox2, or TuJ1 and NICD with DAPI staining in control and *Par3* cKO telencephalons at E11.5. Asterisks indicate regions containing ectopic NPCs. (K,L) Representative immunofluorescence of CldU, IdU and Sox2 in the dorsal region of control and *Par3* cKO littermate telencephalons at E10.5 and E11.5. CldU and IdU were administered 2 and 0.5 h before sacrifice, respectively. Arrowheads and arrows indicate nuclei labeled with only CldU (G2-M) or IdU (early S), respectively. (M,N) Quantification of the nuclear positions labeled with only CldU or IdU at E10.5 and E11.5. Two and three pairs of embryos were analyzed at E10.5 and E11.5, respectively, and the numbers of quantified cells in each embryo are indicated. The boxplots represent the first and third quartiles with thick lines indicating median values. The whiskers represent 1.5 times the interquartile ranges or correspond to the minimum or maximum values. Black circles indicate outliers. Scale bars: 50 μm (A,D,I,J); 20 μm (B,C,E-H,K,L).

Development (2022) 149, dev199931. doi:10.1242/dev.199931

To examine further whether the INM was affected in *Par3* cKO NPCs, we examined the dorsal telencephalon by sequential labeling with two thymidine analogs, 5-chloro-2′-deoxyuridine (CldU) and 5-iodo-2′-deoxyuridine (IdU), at 2 and 0.5 h before sacrifice. As previously demonstrated (Takahashi et al., 1996), we considered that NPCs labeled with CldU, but not IdU, had proceeded to the G2-M phase. In addition, NPCs in early S phase should be labeled by IdU only. Indeed, we readily identified NPCs in different phases of the cell cycle in control and *Par3* cKO dorsal telencephalons at E10.5 and E11.5 (Fig. 3K,L). At E10.5, the nuclei of control NPCs in early S phase were localized away from the ventricle (median distance 38.0 µm; *n*=65) and reached the ventricular surface by the G2-M phase (median distance 13.2 µm; *n*=72), reflecting appropriate INM (Fig. 3K,M). In the control telencephalon at E11.5, alongside the majority of NPCs showing clear INM, a portion of the NPCs in the G2-M phase were distributed away from the ventricle (Fig. 3N, outliers), suggesting the production of intermediate progenitor cells (Noctor et al., 2004). In sharp contrast, *Par3* cKO NPCs at E10.5 were broadly distributed throughout the telencephalon irrespective of whether they were in the early S (median distance 35.1 µm; *n*=95) or G2-M (median distance 20.5 µm; *n*=74) phase (Fig. 3K). We observed further disorganization at E11.5 (Fig. 3L,N), confirming severe INM disturbance in the *Par3* cKO telencephalon. Thus, these results suggest that the perturbed morphology, cell–cell junctions and INM of *Par3* cKO NPCs could be the cause of the histological disorganization of the telencephalon.

Impaired regulation of the self-renewal and differentiation of *Par3* cKO NPCs at the beginning of the neurogenic phase

The above data revealed that many *Par3* cKO NPCs ectopically divided outside the ventricular zone. As shown in Fig. 4A-C, quantitative analysis at E10.5 confirmed that most control NPCs in the dorsal (91.8%, *n*=292/318; median distance 7.7 µm) and ventral (92.1%, *n*=351/381; median distance 7.2 µm) telencephalon divided within 30 µm of the ventricular surface, essentially consistent with a previous report (Fujita et al., 2020). In contrast, significantly fewer *Par3* cKO NPCs divided within 30 µm of the ventricular surface in the dorsal (59.8%, *n*=229/383; median distance 13.8 µm) and ventral (45.6%, *n*=244/535; median distance 45.7 µm) telencephalon. Other peaks of *Par3* cKO NPC divisions were found 75-90 µm away from the ventricle (Fig. 4B,C), representing ectopic NPCs between the neural layers (Figs 2B, 3J).

Production of NPCs away from the ventricle could arise from the altered cleavage plane orientation at the ventricular surface during the expansion and early neurogenic phases (Shitamukai et al., 2011; Yingling et al., 2008). To assess this, we analyzed the cleavage plane orientation of NPC divisions at the ventricular surface at E10.5 (Fig. 4D). Although 72.8% of control NPCs (*n*=49/81) divided at 70-90° to the ventricular surface, significantly fewer NPCs (54.2%, *n*=34/83) divided vertically in the *Par3* cKO telencephalon (Fig. 4E,F). Regarding perturbed cell–cell junctions, these data suggest that the altered cleavage plane orientation at the ventricular surface might also cause the production of ectopic NPCs in the *Par3* cKO telencephalon.

Several studies reported that the orientation of NPC divisions affected the self-renewal and differentiation of their progeny (Fish et al., 2006; Postiglione et al., 2011; Yingling et al., 2008). We therefore performed pulse-chase analysis using BrdU combined with immunofluorescence for self-renewal and differentiation markers, Sox2 and TuJ1, respectively. As previously reported (Takahashi et al., 1995) and observed in our preliminary analysis, the cell-cycle length of NPCs was estimated at more than 8 h in the telencephalon at E10.5. To analyze the fates of NPCs within a single cell cycle, we pulse-labeled pregnant dams at day 10 postcoitum with BrdU 8 h before sacrifice, and then the embryonic telencephalons were co-immunolabeled with BrdU and the fate markers indicated above (Fig. 4G). As shown in Fig. 4H, we clearly identified BrdU-labeled cells positive for Sox2 or TuJ1 (black or white arrowheads, respectively). We also observed single or double layers of TuJ1-positive cells, indicating the beginning of the neurogenic phase. Quantitative analysis of ventral but not dorsal telencephalons revealed a significant increase in the self-renewal activity of *Par3* cKO NPCs (Fig. 4I,J). In ventral telencephalons, control NPCs revealed that single divisions gave rise to 9.9% of differentiated neurons and 90.1% of self-renewing daughter cells (*n*=4 embryos). However, in *Par3* cKO NPCs, the ratio of differentiated neurons was significantly decreased to 6.6%, and that of self-renewing daughters was reciprocally increased to 93.4% (*n*=3 embryos). Because NPCs initially proliferate to self-renew during the expansion phase and then start to differentiate into neurons in the following neurogenic phase, a switch in the balance between self-renewal and differentiation is necessary. Our observations suggest that a larger proportion of *Par3* cKO NPCs maintained self-renewal activity compared with controls at the beginning of the neurogenic phase. Taken together, these findings indicate that PAR3 is required for the appropriate transition of NPCs from the expansion to the neurogenic phase, especially in the ventral telencephalon.

Hyperactivation of hedgehog signaling in *Par3* cKO NPCs

To identify the molecular mechanisms responsible for the observed defects in *Par3* cKO NPCs, we analyzed signaling pathways regulating the self-renewal and differentiation of NPCs, including Notch (Hatakeyama et al., 2004; Shimojo et al., 2008), Shh (Komada et al., 2008; Wang et al., 2016) and canonical Wnt pathways (Hirabayashi et al., 2004; Woodhead et al., 2006). Using quantitative reverse transcription-PCR (RT-qPCR), we analyzed several downstream mRNAs for these pathways in the telencephalon at E10.5. Among the mRNAs examined in Fig. 5A, *Hes5* and *Gli1* were significantly increased in the *Par3* cKO telencephalon, suggesting the activation of Notch and Hh signaling pathways. For confirmation, we analyzed several proteins involved in these pathways in the telencephalon at E11.5 (Fig. 5B-F; Fig. S3). Immunoblotting data, however, did not demonstrate the increased accumulation of activated Notch1, the cleaved intracellular domain (NICD; Fig. 5B), in the *Par3* cKO telencephalon. We also examined Numb protein, a negative regulator of the Notch signaling pathway; however, we found no significant decrease in total Numb protein and no increase in inhibitory phosphorylation in the *Par3* cKO telencephalon (Fig. 5B). In contrast, we consistently found a significantly increased accumulation of Gli1 protein in the *Par3* cKO telencephalon at E11.5 (Fig. 5C,D). Thus, these data demonstrate that Hh signaling is hyperactivated in the *Par3* cKO telencephalon around the beginning of the neurogenic phase. Of note, full-length Gli3 protein (Gli3FL) is primarily processed into a repressor form (Gli3R) and Hh signaling counteracts this conversion to generate a Gli3R gradient along the dorsoventral axis of the telencephalon (Rallu et al., 2002; Wang et al., 2000). Although we found that the ratio between Gli3FL and Gli3R was higher in ventral than dorsal parts, no significant difference was detected between *Par3* cKO and control telencephalons in both parts (Fig. 5E,F). These data suggest that the processing of Gli3FL into Gli3R is not significantly affected in both parts of the *Par3* cKO telencephalon at E11.5.

Development (2022) 149, dev199931. doi:10.1242/dev.199931

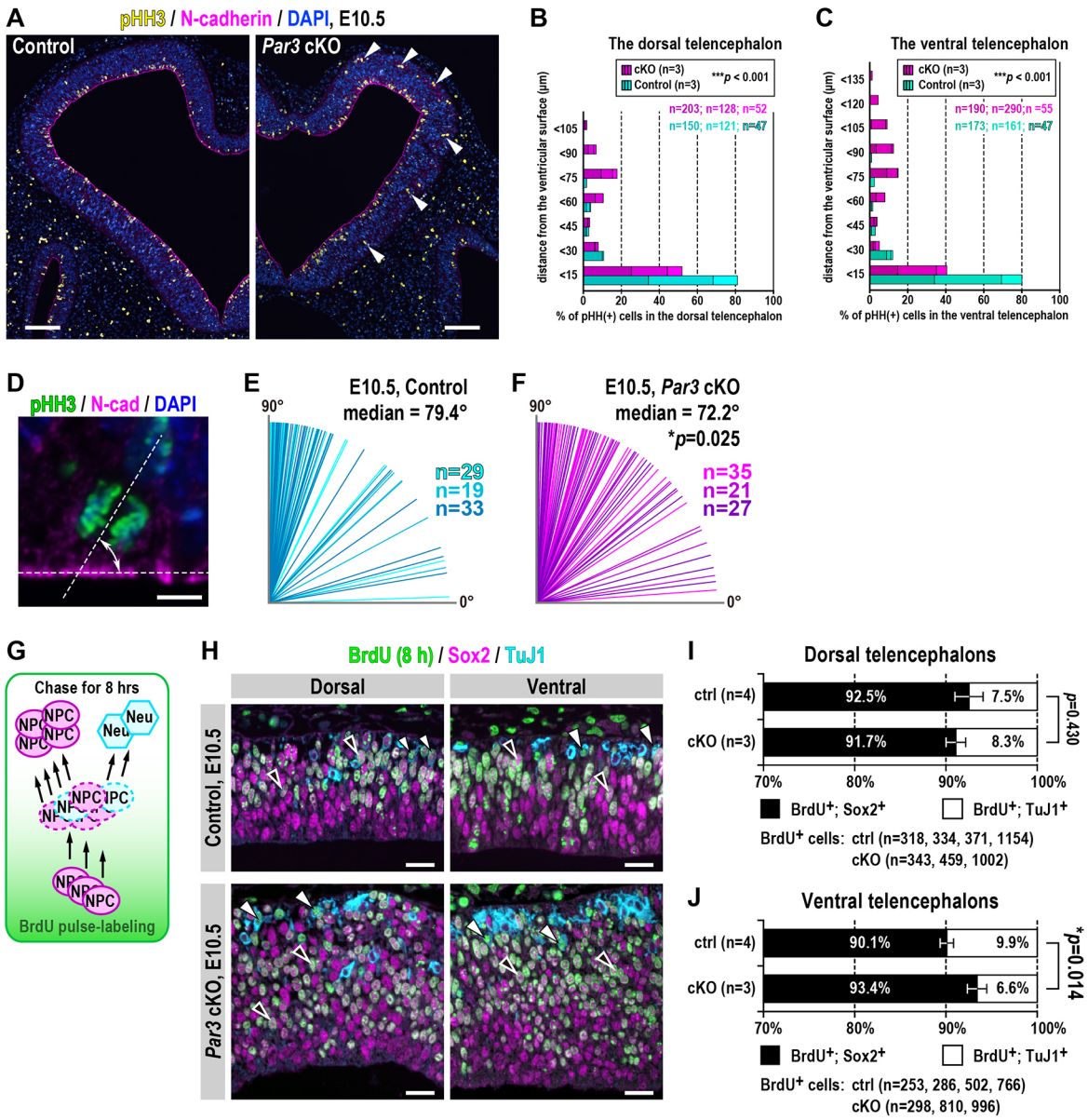

Fig. 4. Loss of PAR3 in NPCs affects the cleavage plane orientation and promotes proliferative divisions. (A) Representative immunofluorescence of phosphorylated histone H3 at Ser10 (pHH3) and N-cadherin (cadherin 2), and DAPI staining in coronal sections of control and *Par3* cKO telencephalons at E10.5 (38 and 35 somites, respectively). Arrowheads indicate ectopic mitotic figures. (B,C) Quantification of the mitotic nuclear positions in dorsal and ventral telencephalons at E10.5. Three embryos were analyzed each for control and *Par3* cKO telencephalons, and the numbers of quantified cells are indicated. (D) A representative mitotic NPC immunolabeled for pHH3 and N-cadherin, and DAPI staining. The angle between the cleavage plane and the ventricular surface (indicated by double-headed arrow) was quantified. (E,F) Quantification of the cleavage plane orientation for mitotic NPCs at the ventricular surface of control and *Par3* cKO telencephalons at E10.5. Three embryos were analyzed for each genotype, and the numbers of analyzed NPCs are indicated. (G) Schematic of the experimental protocol used to analyze the fate of newly divided NPCs. Neu, neuron. (H) Representative immunofluorescence for BrdU labeling 8 h before sacrifice, TuJ1 and Sox2 in control (38 somites) and *Par3* cKO (36 somites) littermate telencephalons at E10.5. Black or white arrowheads indicate BrdU-labeled cells positive for Sox2 or TuJ1, respectively. (I,J) Quantification of the cell fate analysis in four control and three *Par3* cKO telencephalons from two litters at E10.5. The numbers of analyzed $BrdU^+$ nuclei are indicated. The bars and whiskers represent mean values and s.d., respectively. *P*-values were determined with the Brunner–Munzel test (B,C,E,F) or two-tailed Welch's *t*-test (I,J). Scale bars: 100 µm (A); 5 µm (D); 20 µm. (H).

Next, we clarified how Hh signaling was compromised in *Par3* cKO NPCs. To achieve this, we took advantage of primary neurosphere cultures to expand NPCs exclusively (Nagao et al., 2008; Reynolds and Weiss, 1996), and inhibited Hh signaling with SANT-1, a direct Smo antagonist (Chen et al., 2002) (Fig. 5G). We prepared primary neurospheres from *Par3* cKO and control telencephalons at E11.5 and treated them with various concentrations of SANT-1 for 1 day. RT-qPCR analysis revealed a significant increase in mRNAs of the downstream targets of Hh signaling, *Gli1* and *Ptch1*, but not those of upstream molecules, in the neurospheres derived from the *Par3* cKO telencephalon (Fig. 5H). These results indicate that neurospheres faithfully mimic the hyperactivation of Hh signaling observed *in vivo*. Of note, *Hes5* mRNA was not significantly changed in the *Par3* cKO neurospheres, suggesting that increased *Hes5* mRNA detected in whole telencephalons (Fig. 5A) might have resulted from a higher proportion of NPCs in *Par3* cKO telencephalons than controls at E10.5. Treatment of *Par3* cKO neurospheres with 5 nM SANT-1, a

Development (2022) 149, dev199931. doi:10.1242/dev.199931

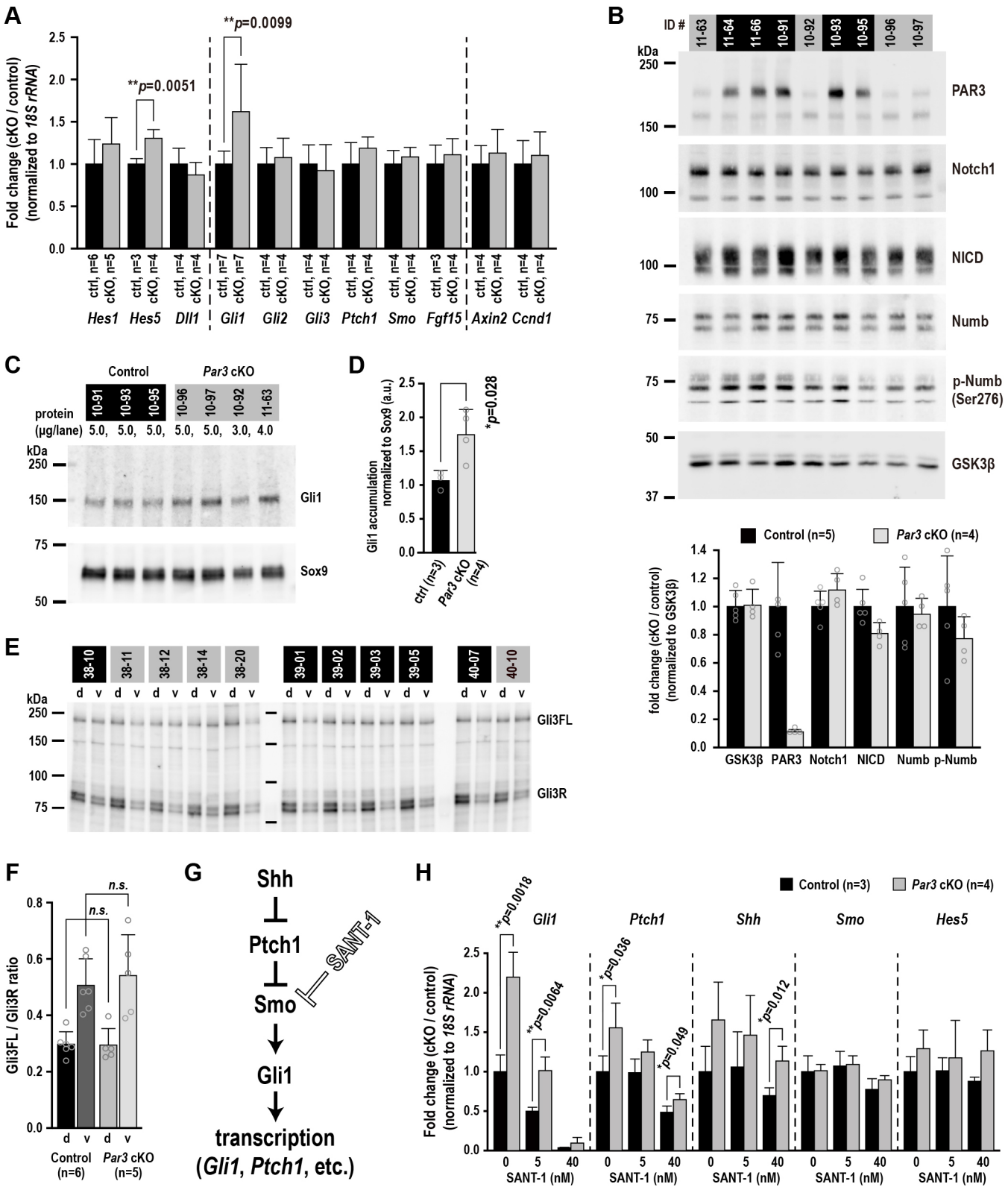

Fig. 5. Loss of PAR3 in NPCs results in hyperactivation of Hh signaling. (A) RT-qPCR analyses for the indicated mRNAs in dissected telencephalons at E10.5. The numbers of analyzed embryos are indicated. (B-F) Immunoblot analysis of the indicated proteins in dissected whole (B-D), dorsal (d) and ventral (v) (E,F) telencephalons at E11.5. GSK3β or Sox9 were used as loading controls. The IDs of control and *Par3* cKO embryos are labeled in white and black, respectively. The genotypes of control embryos are *Foxg1*$^{+/Cre}$;*Par3*$^{\Delta E3/+}$ (39-01, 39-02, 39-03, 39-05) or *Foxg1*$^{+/Cre}$;*Par3*$^{floxE3/+}$ (the others). (G) SANT-1 directly binds to and inhibits Smo in the Hh signaling pathway. (H) RT-qPCR analyses of primary cultured neurospheres derived from telencephalons of three control and four *Par3* cKO embryos at E11.5. Neurospheres on day 3 were incubated for 24 h with vehicle (DMSO) or SANT-1 at the indicated concentrations. The bars and whiskers in all graphs represent mean values and s.d., respectively. *P*-values were determined by the two-tailed Welch's *t*-test. n.s., not significant.

Development (2022) 149, dev199931. doi:10.1242/dev.199931

much lower concentration than the IC50 (20 nM) used in previous reporter assay studies (Chen et al., 2002), inhibited the accumulation of *Gli1* mRNA to a level similar to that observed in control neurospheres without SANT-1. Moreover, treatment with 40 nM SANT-1 almost completely blocked *Gli1* mRNA accumulation in both neurospheres, consistent with the Smo-dependent autoregulatory function of Gli1 transcription factor (Vokes et al., 2007). This contrasts with a previous report showing that aPKC phosphorylated Gli1 and enhanced DNA-binding activity to induce *Gli1* transcription by itself in a Smo-independent manner (Atwood et al., 2013); aPKC forms an evolutionarily conserved complex with PAR3 that is required for controlling cell polarity (Ohno et al., 2015). Treatment with SANT-1 similarly inhibited, but did not completely block, the accumulation of *Ptch1* mRNA in the *Par3* cKO neurospheres. Although we did not detect a significantly increased accumulation of *Ptch1* mRNA in the *Par3* cKO telencephalon at E10.5, the results in neurospheres derived from telencephalons at E11.5 suggest that the accumulation of *Ptch1* mRNA might be followed by increased *Gli1* mRNA expression (Fig. 5G). These observations reveal that Smo activity is required for the hyperactivation of Hh signaling in *Par3* cKO NPCs.

PAR3 is required for ciliary integrity to restrict smoothened in primary cilia

Next, we investigated which step in Hh signaling was compromised in the *Par3* cKO telencephalon. Although we assessed the expression pattern and intensity of Shh in the ventral telencephalons at E10.5, we did not observe any difference between *Par3* cKO and control embryos (Stoykova et al., 2000) (Fig. S4A,B). Staining of NPCs for several marker proteins of dorsoventral telencephalic regions confirmed the establishment of sharp pallial-subpallial boundaries in *Par3* cKO and control telencephalons at E11.5 (Englund, 2005; Guillemot and Joyner, 1993; Toresson et al., 2000) (Fig. S4C-F). Next, we focused on Ptch1 and Smo in primary cilia. In vertebrates, although cilia-localized Ptch1 excludes Smo, Shh binding to Ptch1 allows Smo to be localized to cilia and activate downstream Hh signaling (Fig. 6K) (Bangs and Anderson, 2017; Corbit et al., 2005; Rohatgi et al., 2007). In addition, PAR3 is required for the biogenesis of primary cilia in cultured epithelial cells (Sfakianos et al., 2007). Therefore, we examined primary cilia in the apical domain of NPCs that comprise the ventricular surface of the telencephalon by finite super-resolution confocal microscopy at E10.5 (Borlinghaus and Kappel, 2016). In control ventricles, en face images demonstrated that many primary cilia had an elongated club-like shape with a neck and were associated with the basal bodies in NPCs (Fig. 6A). Although every *Par3* cKO NPC developed primary cilia associated with the basal bodies, we found many shorter cilia without apparent necks (Fig. 6B). Quantitative analysis supported the observation that the primary cilia in *Par3* cKO NPCs were significantly shorter than those in controls (median length 1.01 µm versus 1.12 µm; n=211 versus n=152; Fig. 6C). Scanning electron microscopy demonstrated further that many *Par3* cKO NPCs had shorter and bullet-shaped primary cilia, whereas most control NPCs had an elongated club-like shape with a neck (Fig. 6D,E). These observations suggest that the integrity of the primary cilia is compromised in *Par3* cKO NPCs.

Even subtle defects in ciliary integrity have been reported to possibly result in the activation or inhibition of Hh signaling (Bangs and Anderson, 2017). The hyperactivation of Hh signaling can be caused by the ciliary exclusion of Ptch1 and/or a dysregulated ciliary concentration of Smo. To assess whether the ciliary regulation of Hh signaling depends on PAR3, we examined the ciliary localization of YFP-tagged Ptch1 and Smo (Milenkovic et al., 2009; Rohatgi et al., 2007) in Flp-In 3T3 cell lines expressing each protein via site-specific recombination into the single Flp recombination target site (Dorn et al., 2012). Immunoblotting and immunofluorescence analyses revealed a reduction of PAR3 by transient transfection with two independent siRNAs in the established Flp-In-3T3/Ptch1-YFP and Flp-In-3T3/YFP-Smo cell lines (Fig. 6F,G,I). Serum-starvation for 18 h with 0.5% calf serum successively induced the formation of primary cilia (Schneider et al., 2005) in cell lines transfected with the non-silencing control (NS Ctrl) or *Par3*-targeting siRNAs (Fig. 6G,I). As previously reported (Rohatgi et al., 2007), Ptch1-YFP localized to the tips and bases of primary cilia in Flp-In-3T3/Ptch1-YFP cells transfected with NS Ctrl siRNA (Fig. 6G). Two independent siRNAs targeting *Par3* did not consistently diminish this localization pattern or the concentration of Ptch1-YFP in primary cilia (Fig. 6G,H; Fig. S5E). In addition, stimulation of these cells with 20 nM of recombinant Shh-N C24II mutant, which is eightfold more potent than wild-type Shh (Taylor et al., 2001), similarly reduced the ciliary localization of Ptch1-YFP irrespective of the transfected siRNA (Fig. S5A-D). Together with the observations showing high *Ptch1* mRNA accumulation in the *Par3* cKO neurospheres (Fig. 5E), these data suggest that the loss of PAR3 does not hyperactivate Hh signaling by impacting Ptch1 activity.

Finally, we assessed the ciliary localization of YFP-Smo following the reduction of PAR3. As expected (Milenkovic et al., 2009), few control cells displayed ciliary localization of YFP-Smo without stimulation (Fig. 6I; Fig. S5F; NS Ctrl). In contrast, two independent siRNAs targeting *Par3* significantly increased ciliary accumulation of YFP-Smo without stimulation (Fig. 6I,J; Fig. S5F; *Par3* RNAi/H2, M2). Notably, stimulation with 10 nM SAG1.3, a direct agonist of Smo (Chen et al., 2002), induced greater accumulation of YFP-Smo in these cells irrespective of the transfected siRNA (Fig. S5G-I). Collectively, these findings demonstrate that PAR3 has a crucial role in restricting ciliary Smo localization to regulate Hh signaling through the establishment of ciliary integrity (Fig. 6K). To confirm this idea *in vivo*, we compared ciliary Smo intensities between *Par3* cKO and control telencephalons at E11.5. We employed finite super-resolution confocal microscopy to quantitatively observe ciliary Smo with IFT88, a ciliary marker protein used as a control (Pazour et al., 2002) (Fig. 7A). In dorsal and ventral ventricles, we detected significantly higher Smo intensities in primary cilia of *Par3* cKO telencephalons than controls at E11.5 (Fig. 7B). These data suggest that PAR3 is required for the appropriate exclusion of Smo from primary cilia in the telencephalon.

To address whether the hyperactivation of Hh signaling has a causative role in the phenotypes observed in the *Par3* cKO telencephalon, we injected cyclopamine, a direct Smo inhibitor, or vehicle alone to pregnant dams at day 9.5 postcoitum, and then analyzed embryonic telencephalons at E10.5 (Chen et al., 2002; Incardona et al., 1998; Palma and Ruiz i Altaba, 2004). We confirmed the successful but partial inhibition of Hh signaling by cyclopamine in the limb buds of embryos by RT-qPCR for *Gli1* mRNA (Fig. 7C). Immunofluorescence of phosphorylated histone H3 at Ser10 and BrdU pulse-labeled 30 min before sacrifice revealed that the proportion of NPCs in M phase was significantly decreased by cyclopamine in *Par3* cKO dorsal telencephalons (mean 10.9% versus 13.1%, n=3 embryos each; Fig. 7D,E) to a level similar to that in control embryos treated with vehicle (mean 10.4%,

Development (2022) 149, dev199931. doi:10.1242/dev.199931

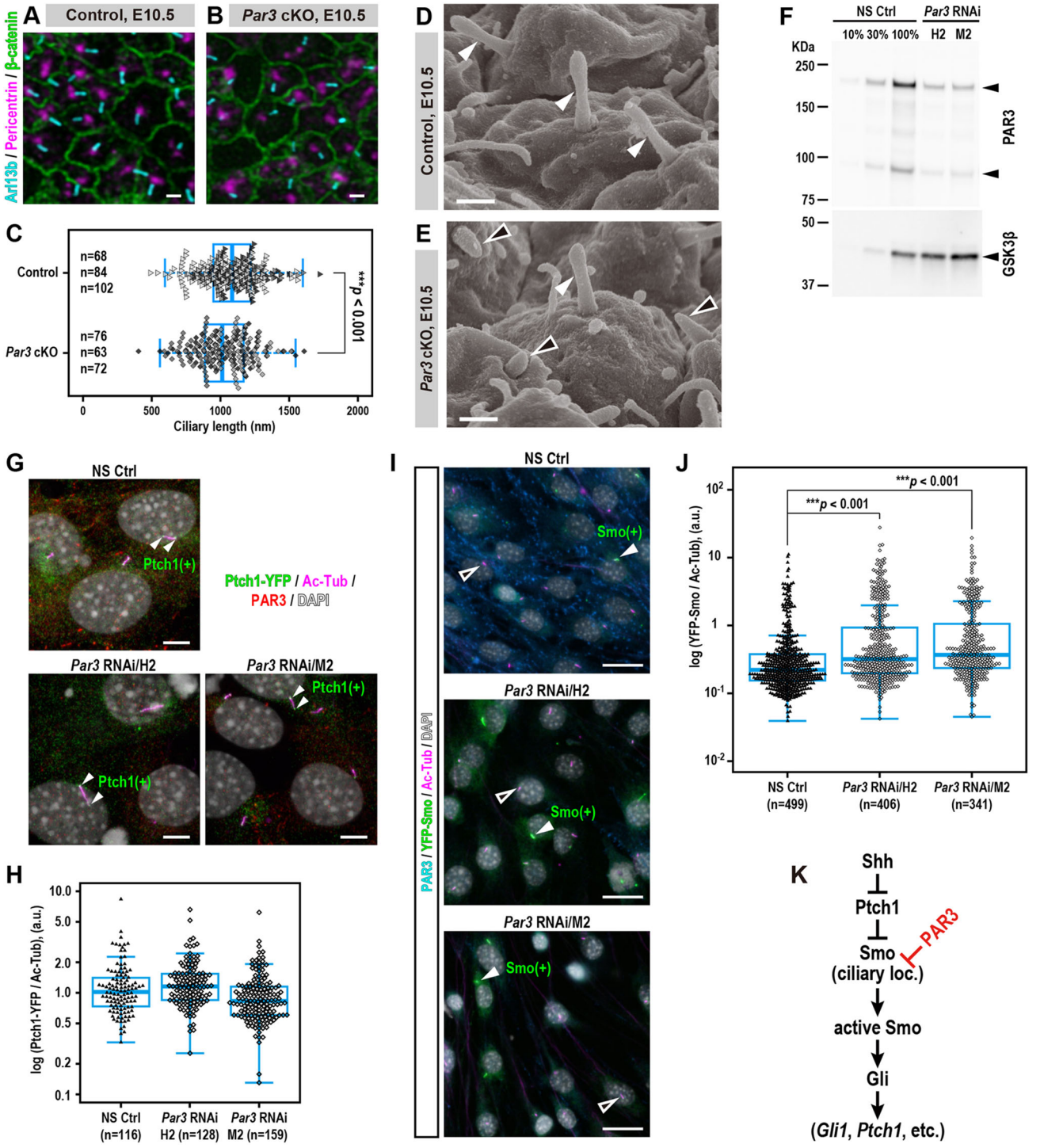

Fig. 6. Loss of PAR3 perturbs ciliary integrity and leads to dysregulated localization of Smo in primary cilia. (A,B) Representative whole-mount immunofluorescence of Arl13b, pericentrin and β-catenin in control (35 somites) and *Par3* cKO (36 somites) littermate telencephalons at E10.5. Finite super-resolution confocal images were acquired en face, and maximal intensity projection images were prepared from deconvoluted images. (C) Quantification of ciliary length in telencephalons of three pairs of control and *Par3* cKO embryos from four independent litters at E10.5. The numbers of quantified cilia are indicated. (D,E) Representative scanning electron microscopy of the ventricular surface of control and *Par3* cKO littermate (32 somites each) telencephalons at E10.5. White and black arrowheads indicate bottle neck-like and bullet-shaped cilia, respectively. (F) Immunoblotting of PAR3 in Flp-In-3T3/Ptch1-YFP cells transfected with the indicated siRNAs. Arrowheads indicate the PAR3 isoforms expressed in fibroblasts. GSK3β was used as a loading control. (G,I) Immunofluorescence of PAR3, YFP and acetylated α-tubulin, and DAPI staining in Flp-In-3T3/Ptch1-YFP (G) or Flp-In-3T3/YFP-Smo cells (I) transfected with the indicated siRNAs. (H,J) Quantification of the ciliary intensity of Ptch1-YFP (H) or YFP-Smo (J) in each group of cells transfected with the indicated siRNAs. The cilia on PAR3-negative cells were analyzed for *Par3* RNAi/H2 and M2 cells. (K) PAR3 restricts the ciliary localization of Smo in the Hh signaling pathway. Boxplots represent the first and third quartiles with thick lines indicating median values (C,H,J). The whiskers represent 1.5 times the interquartile ranges or correspond to the minimum or maximum values. The Brunner–Munzel test was used to determine *P*-values (C,J). Scale bars: 1 µm (A,B); 500 nm (D,E); 5 µm (G); 20 µm (I).

Development (2022) 149, dev199931. doi:10.1242/dev.199931

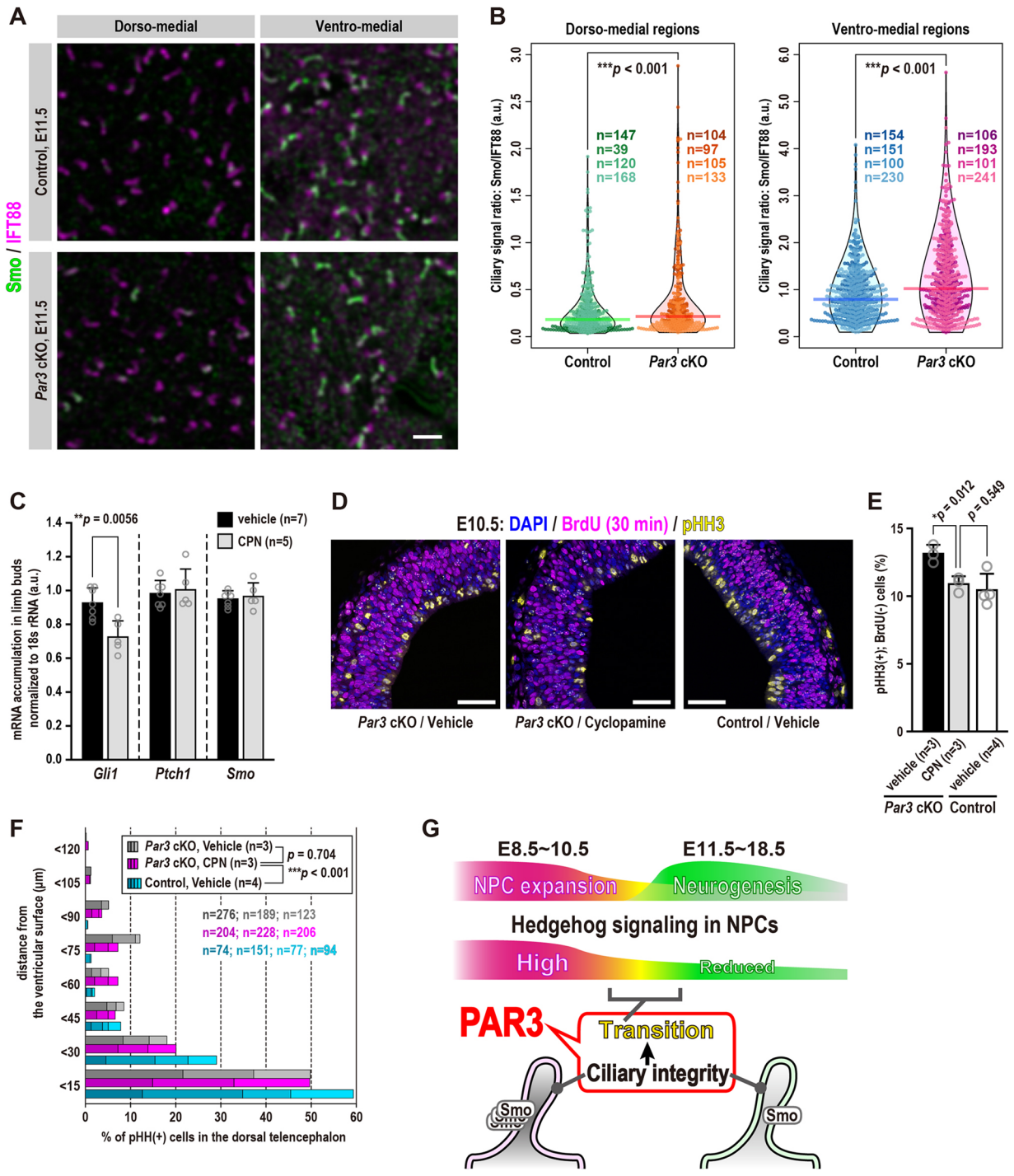

Fig. 7. Hyperactivation of Smo activity promotes increased NPC proliferation in the *Par3* cKO telencephalon. (A) Representative whole-mount immunofluorescence of Smo and IFT88 in control and *Par3* cKO telencephalons at E11.5. Finite super-resolution confocal images were acquired en face, and ciliary signals are shown in deconvoluted single slices. Scale bar: 2 µm. (B) Quantification of the ciliary accumulation of Smo in telencephalons of four control and *Par3* cKO embryos each. Dorsal and ventral parts were separately analyzed, and the numbers of analyzed cilia are indicated. Horizontal lines represent median values. (C) RT-qPCR analyses for the indicated mRNAs in limb buds of *Par3* cKO embryos treated with cyclopamine (CPN) or vehicle alone. The numbers of analyzed embryos are indicated. (D) Representative immunofluorescence of phosphorylated histone H3 at Ser10 and pulse-labeled BrdU, and DAPI staining in coronal sections of the dorsal telencephalon of *Par3* cKO embryos with or without cyclopamine treatment and a control embryo at E10.5 (34, 32 and 34 somites, respectively) treated with the indicated reagents. Scale bars: 50 µm. (E,F) Quantification of mitotic cells (E) and nuclear positions (F) in dorsal parts of *Par3* cKO and control telencephalons at E10.5 treated with CPN or vehicle alone. Each of three *Par3* cKO and four control embryos was used to analyze 737-2227 cells per embryo (E) or the numbers of cells indicated (F). *P*-values were determined by the Brunner–Munzel test (B,F) or two-tailed Welch's *t*-test (C,E). (G) Schematic of the role of PAR3 in the transition of NPCs from the expansion to the neurogenic phase. Mouse telencephalic NPCs exclusively proliferate at approximately E8.5-E10.5 (expansion phase) and shift to produce neurons at approximately E11.5-E18.5 (neurogenic phase). Hh signaling activity is maintained at a high level in the expansion phase, whereas it is reduced in the following neurogenic phase. PAR3 restricts Hh signaling in NPCs through the establishment of ciliary integrity to induce the transition from the expansion to the neurogenic phase at the proper developmental time.

Development (2022) 149, dev199931. doi:10.1242/dev.199931

n=4 embryos). However, the proportions of ectopic NPCs were not significantly altered by cyclopamine (Fig. 7F), suggesting that this phenotype was not as sensitive as the proliferation measure, or that many NPCs were already detached from the ventricle by E9.5. Nonetheless, these observations support the idea that the Smo-dependent hyperactivation of Hh signaling increases NPC proliferation in the *Par3* cKO telencephalon.

DISCUSSION

During brain development, the final number of neurons is highly dependent on the size of the NPC pool at the onset of neurogenesis. Thus, the timing of the transition from the proliferative to the neurogenic division phase is tightly controlled in NPCs (Miyata et al., 2010; Rakic, 1995; Taverna et al., 2014). Here, we demonstrated that PAR3 is required for this appropriate transition by restricting proliferative NPC divisions during early telencephalic development, especially in the ventral region. Moreover, PAR3 has crucial roles in the regulation of ciliary integrity and the repression of Smo activity in primary cilia. These observations support the idea that PAR3 restricts Hh signaling in NPCs to induce the transition from the expansion to the neurogenic phase for proper development of the telencephalon (Fig. 7G).

The *Par3* cKO telencephalon and primary cultured NPCs showed robust activation of Hh signaling (Fig. 5A,C,E). Consistent with the effect of Hh signaling on the proliferation of several types of NPCs, including those in dorsal and ventral telencephalon (Komada et al., 2008; Matsumoto et al., 2020; Wang et al., 2016), we demonstrated that the hyperactivation and hyperproliferation in *Par3* cKO NPCs depends on Smo activity (Figs 5E, 7E). We further showed the requirement of PAR3 to restrict ciliary localization of Smo in the telencephalon (Fig. 7B). On the basis of these findings, along with our observations demonstrating defective ciliary development in *Par3* cKO NPCs (Fig. 6B,E), we propose that PAR3 restricts Hh signaling by establishing ciliary integrity in NPCs in the developing telencephalon, thereby controlling ciliary Smo localization (Fig. 7G). This is consistent with previous reports demonstrating crucial roles of PAR3 in the biogenesis of the primary cilium and the establishment of apical domain integrity in several types of polarized cells (Hirose et al., 2006; Horikoshi et al., 2009; McCaffrey and Macara, 2009; Sfakianos et al., 2007). In particular, molecular interaction between PAR3 and KIF3a, a subunit of the anterograde kinesin-2 motor complex, has been shown to be required for ciliary development in MDCK cells (Sfakianos et al., 2007). Because ciliary Smo localization was induced by Shh-dependent association with KIF3a (Kovacs et al., 2008), it is plausible that PAR3 competes with Smo for association with KIF3a, thereby restricting ciliary Smo localization.

Previous studies in mouse NPCs indicate that PAR3 promotes neurogenic divisions during the early neurogenic phase and proliferative divisions in the mid-neurogenic phase, in a developmental stage-specific manner (Bultje et al., 2009; Costa et al., 2008; Liu et al., 2018). In this study, two different *Par3* mutant mouse lines (*Foxg1*$^{+/Cre}$;*Par3*$^{\Delta E3/floxE3}$ and *NesCre*$^{Tg+}$;*Par3*$^{\Delta E3/floxE3}$) were used to extend our knowledge of the stage-specific roles of PAR3 in NPC proliferation (Fig. 2). In particular, our results reveal that PAR3 is required for the restriction of NPC proliferation to a narrow time window to permit neurogenic division for the appropriate transition from the expansion to the neurogenic phase (Fig. 7G). Because a limited number of molecules have been shown to be involved in this phase transition, the function of PAR3 sheds new light on the basic mechanisms underlying the development of the telencephalon.

Analyses of several mouse mutants and human ciliopathies revealed that primary cilia in NPCs are required for cerebral development by controlling apicobasal cell polarity, mitotic spindle orientation, proliferation and differentiation (Guemez-Gamboa et al., 2014; Liu et al., 2021; Willaredt et al., 2013). Moreover, it was shown that some ciliary proteins, including Arl13b, KIF3a and IFT88, have crucial roles in brain development, particularly before the neurogenic phase (Higginbotham et al., 2013; Snedeker et al., 2017; Tong et al., 2014; Wilson et al., 2012). Previous (Liu et al., 2018) and current results are in intriguing agreement with the stage-specific function of PAR3 in the regulation of NPC proliferation during similar developmental stages. This suggests that a mechanism involving PAR3 in primary cilia might also be involved in the transition from the expansion to the neurogenic phase during neurogenesis.

Recent studies have indicated that the generation of various types of NPCs during telencephalic development involved several cellular mechanisms, including the regulation of apical cell–cell junctions, INM, and cleavage plane orientations (LaMonica et al., 2012; Matsuzaki and Shitamukai, 2015; Taverna et al., 2014). In particular, increased oblique cleavage plane orientations enhanced the production of OSVZ progenitors during the development of mouse and ferret telencephalons (Martínez-Martínez et al., 2016; Shitamukai et al., 2011). We observed dysregulation of INM and cleavage plane orientations (Figs 3K-N, 4D-F), as well as the overproduction of self-renewing NPCs dividing away from the ventricle (Figs 3D-J, 4A-C). Considering that these characteristic phenotypes are induced by deletion of the *Par3* gene in a stage-dependent manner, our observations imply that hypertrophy in the *Par3* cKO telencephalon resulted from the enhanced production of OSVZ progenitor-like cells during a specific developmental time window. This hypothesis is supported by previous reports showing that human and ferret OSVZ progenitors lost PAR3 expression (Fietz et al., 2010), and that *Par3* mRNA expression in the ventricular zone tended to be downregulated concomitant with the transient peak of OSVZ progenitor production during ferret telencephalic development (Martínez-Martínez et al., 2016). Indeed, we observed *Par3* cKO NPCs with OSVZ progenitor-like morphology (Fig. 3H) and the expression of marker proteins, including Sox2, NICD and Pax6 (Fig. 3J; Fig. S4D), in the telencephalon. Furthermore, the possible expansion of OSVZ progenitor-like cells with hyperactivation of Hh signaling is in line with previous reports demonstrating that increased Hh signaling was sufficient to expand self-renewing OSVZ progenitors and cause hypertrophy in the mouse and ferret neocortex (Matsumoto et al., 2020; Wang et al., 2016).

Taken together, our findings reveal crucial roles for PAR3 in the transition of NPCs from the expansion to the neurogenic phase during a limited developmental period by regulating Hh signaling, especially in the ventral region. Further investigations of the *Par3* cKO telencephalon should clarify the mechanisms regulating the initial expansion of the NPC pool, as well as the production of OSVZ progenitors.

MATERIALS AND METHODS

Reagents

We obtained BrdU (027-15561), IdU (094-01761) and 2-hydroxypropyl-beta-cyclodextrin (HPβCD, 326-84232) from Wako Pure Chemicals, SANT-1 (559303) and SAG1.3 in solution (566661) from EMD Millipore, CldU (C6891) and 5-bromo-4-chloro-3-indolyl β-D-galactopyranoside (X-gal, B4252) from Sigma-Aldrich, and recombinant human Shh (C24II, 130-095-727) from Miltenyi Biotec. A stock solution of cyclopamine (C-8700, lot BAC-117, LC Laboratories) was produced at 25 mg/ml in ethanol and a solution for injection at 1 mg/ml was prepared in PBS(–) containing 45% HPβCD with agitation every 10 min at 65°C.

Development (2022) 149, dev199931. doi:10.1242/dev.199931

Animals

All mouse experiments were conducted in accordance with the Guidelines for Proper Conduct of Animal Experiments (Science Council of Japan), and all protocols were approved by our institutional review boards. We used the mouse lines listed in Table S1 to obtain *Par3* cKO (*Foxg1*$^{+/Cre}$;*Par3*$^{\Delta E3/floxE3}$), *Nestin-Cre*-mediated *Par3* mutant (*NesCre*$^{Tg+}$;*Par3*$^{\Delta E3/floxE3}$) and control (*Foxg1*$^{+/Cre}$;*Par3*$^{+/floxE3}$ or *NesCre*$^{Tg+}$;*Par3*$^{+/floxE3}$) embryos (Hébert and McConnell, 2000; Hirose et al., 2006; Iden et al., 2012; Imai et al., 2006).

To obtain embryonic stem cell (ESC) clones harboring the *Par3*^{floxE3} allele but not the floxed Neo^{R} cassette in the *Par3*^{Neo} allele, the previously established *Par3*$^{Neo/+}$ ESC clone #38 (Hirose et al., 2006) was electroporated with pCre-PAC (Taniguchi et al., 1998) to transiently express Cre recombinase and puromycin N-acetyltransferase. ESC clones harboring the *Par3*^{floxE3} allele without Cre gene integration were screened by PCR and Southern blot analysis, and then injected into C57BL/6J blastocysts to obtain chimeric mice. The chimeric males were crossed to C57BL/6J females (CLEA Japan) and germline transmission of the *Par3*^{floxE3} allele was confirmed by genomic Southern blotting. We also bred *Par3*$^{\Delta E3/+}$ (Hirose et al., 2006) mice with *Foxg1-Cre* mice (Hébert and McConnell, 2000) to generate *Foxg1*$^{+/Cre}$;*Par3*$^{\Delta E3/+}$ mice. The established founder mouse lines were backcrossed to 129X1/SvJ mice (The Jackson Laboratory) for three generations to achieve tissue-specific Cre expression (Hébert and McConnell, 2000). These mouse lines (*Par3*$^{floxE3/floxE3}$ and *Foxg1*$^{+/Cre}$;*Par3*$^{+/\Delta E3}$ mice) were then bred to obtain *Par3* cKO (*Foxg1*$^{+/Cre}$;*Par3*$^{floxE3/\Delta E3}$) and control (*Foxg1*$^{+/Cre}$;*Par3*$^{floxE3/+}$) embryos. All mice were housed under a 12-h light/dark cycle with access to water and standard chow *ad libitum*.

Primer sets used to genotype *Par3* or *Foxg1-Cre* mice are listed in Table S3. For the *Par3* gene, Par3/-423iF, Par3/0509R and Par3/+598iR primers generated products of 484 bp for wild type, 563 bp for the E3-floxed allele, and 292 bp for the ΔE3 allele. For the *Foxg1* gene, Bf1–F25, Bf1–R159, and NCre+243R primers gave products of 186 bp for wild type and 265 bp for the Cre knock-in allele (Muzio and Mallamaci, 2005). *ROSA26* Cre reporter mice (The Jackson Laboratory) were genotyped according to a previous report (Soriano, 1999). The *Nestin-Cre* transgene containing a neuroepithelial enhancer was detected by the presence of a 325-bp product using the Enes+233iF and Enes+557iR primers for the second intron of the rat nestin gene (Imai et al., 2006; Zimmerman et al., 1994).

For pulse-labeling with thymidine analogs, pregnant dams were intraperitoneally injected with BrdU, IdU and CldU at 165 nmol/g. Stock solutions of BrdU and CldU or IdU were prepared at 16.5 nmol/µl in PBS(–) or 10% DMSO/PBS(–), respectively. To inhibit Smo in embryos, pregnant dams were intraperitoneally injected with cyclopamine at 10 µg/g 24 h before sampling at E10.5 (Palma and Ruiz i Altaba, 2004).

Immunoblotting

Dissected whole, dorsal or ventral telencephalons at E10.5 or E11.5 were lysed in 20 mM HEPES-NaOH (pH 7.5), 150 mM NaCl, 0.1% SDS and 1.0% Triton X-100, supplemented with 1.0% each of protease and phosphatase inhibitor cocktails (P8340 and P5726, Sigma-Aldrich), and subjected to immunoblotting with the following antibodies: anti-PAR3 pAb (0.5 µg/ml), anti-Notch1 (2.0 µg/ml), anti-cleaved-Notch1 (1/1000), anti-Numb (1/1000), anti-p-Numb (1/1000), anti-GSK3β (0.25 µg/ml), anti-Gli1 (1/250), anti-Sox9 (0.5 µg/ml), anti-Gli3 (1.0 µg/ml) and anti-Nkx2.1 (1.0 µg/ml) (see Table S2). The chemiluminescent signals from the corresponding secondary antibodies were captured with a luminoimage analyzer (LAS-4000IR, Fujifilm) using ImmunoStar LD (292-69904, Wako Pure Chemicals) for Gli1 or Immobilon Western (WBKLS0500, Millipore) for the other proteins. The results of immunostaining were analyzed using Multi Gauge software (v2.2, Fujifilm). Statistical analyses to compare each pair of results were performed using the two-tailed Welch's *t*-test using R statistical software (R Foundation for Statistical Computing; Table S4).

Immunofluorescence

For cryosections, dissected embryos were fixed in 1% (w/v) trichloroacetate (TCA; 4°C, 30 min), 4% paraformaldehyde (PFA)/PBS (4°C, 3-4 h), or PFA-lysine-periodate fixative (PLP; 2 h, 4°C) (McLean and Nakane, 1974), cryoprotected through increasing concentrations of sucrose up to 30% in PBS at 4°C, and then embedded in 67% Tissue-Tek O.C.T. compound (Sakura Finetek Japan) and 10% sucrose in PBS. For paraffin sections, embryos were fixed in Bouin's fixative (3 h, 4°C) or 4% PFA/PBS (4°C, overnight), dehydrated, and embedded in paraffin wax. The cryosections and paraffin sections were processed for heat-induced epitope retrieval (HIER) using target retrieval solution (S1700, Dako/Agilent Technologies) at 105 or 121°C for 15 min for anti-BrdU/IdU (0.5 µg/ml), anti-BrdU/CldU (2.5 µg/ml) and anti-integrin β1 (2.0 µg/ml) monoclonal antibodies (mAbs), or anti-PAR3 (2.0 µg/ml), anti-phospho-histone H3 (1.0 µg/ml) and anti-Sox2 (4.0 µg/ml) polyclonal antibodies (pAbs), respectively. HIER was not used for the following: anti-PAR3 (ascites, 1/100) and anti-ZO-1 (0.5 µg/ml) mAbs in TCA-fixed cryosections; anti-pericentrin (1.0 µg/ml), anti-phospho-vimentin (1.0 µg/ml), anti-Sox2 (1.0 µg/ml), anti-N-cadherin (1.0 µg/ml), anti-aPKCλ (2.5 µg/ml), anti-nestin (5.0 µg/ml), anti-Shh (1.0 µg/ml), anti-Pax6 (2.0 µg/ml) mAbs, anti-β-catenin (0.2 µg/ml), anti-phospho-histone H3 (1.0 µg/ml), anti-TTF1/Nkx2-1 (1.0 µg/ml) and anti-Gsh2 (1/500) pAbs in PLP-fixed cryosections; and anti-βIII-tubulin mAb (0.5 µg/ml) in paraffin sections. We used a biotin-free tyramide-fluorescein signal amplification system with peroxidase-conjugated anti-fluorescein (CSAII kit and CSAII Rabbit Link, K1497 and K1501, Dako) with rabbit anti-cleaved Notch1 mAb (1/500). For whole-mount immunofluorescence, PLP-fixed telencephalons were incubated with anti-Arl13b (2.0 µg/ml) and anti-pericentrin (2.0 µg/ml) mAbs, and anti-β-catenin pAb (0.5 µg/ml), or anti-Smoothened mAb (5.0 µg/ml) and anti-IFT88 pAb (2.0 µg/ml). Flp-In-3T3/Ptch1-YFP or Flp-In-3T3/Smo-YFP fibroblasts were fixed in 2% PFA/PBS for 10 min at room temperature for anti-PAR3 (2.0 µg/ml) and anti-GFP (2.0 µg/ml) pAbs, and anti-acetylated-α-tubulin mAb (ascites, 1/1000). The primary antibodies were visualized using corresponding secondary antibodies (1.0-2.0 µg/ml). Details of all the antibodies used are given in Table S2. Sections were counterstained with 4′,6-diamidino-2-phenylindole dihydrochloride (DAPI), and mounted in ProLong Gold or ProLong Glass Antifade Mountant (P36930 or P36984, Thermo Fisher Scientific).

Fluorescent images were acquired using an epifluorescence microscope (BX50, Olympus) equipped with a CCD camera (Sensys 1400-G2, Teledyne Photometrics), a laser-scanning confocal microscope system (Axioimager Z1 with LSM700, Carl Zeiss), or a spinning-disk confocal microscope system (Axioimager Z1, Carl Zeiss; CSU10, Yokogawa Electric Corporation; ORCA-R2, Hamamatsu Photonics). Finite super-resolution images were acquired on a confocal microscope system (TCS SP8 with HyD, Leica Microsystems) with a ×100 objective lens (HC PL APO CS2×100/1.40 NA OIL) with a pinhole of 0.5 Airy unit diameter (Borlinghaus and Kappel, 2016). The *xy*- and *z*-sampling rates were respectively set to 22.7 and 80 nm, or 45.5 and 150 nm, and acquired images were deconvoluted using Huygens Professional software (Scientific Volume Imaging). Images were processed, arranged and labeled using ImageJ (Schneider et al., 2012) (NIH), Photoshop CS5 (v12.0 x64, Adobe) and Illustrator CS5 (v15.0.0, Adobe).

Immunohistochemistry and histology

Paraffin sections (2 µm thick) were subjected to immunohistochemistry using the primary monoclonal antibodies anti-BrdU/IdU (0.5 µg/ml) and anti-βIII-tubulin (0.5 µg/ml). Biotinylated secondary antibodies (1.0 µg/ml, anti-mouse IgGs) were visualized using a VECTASTAIN Elite ABC kit (PK-6100, Vector Laboratories; RRID: AB_2336819) with 3,3′-diaminobenzidine (DAB) as a substrate and counterstained with Carazzi's Hematoxylin (30021, Muto Pure Chemicals). We utilized a biotin-free tyramide-fluorescein signal amplification system with peroxidase-conjugated anti-fluorescein (CSAII kit and CSAII Rabbit Link, K1497 and K1501, Dako) for anti-Mash1/Ascl1 mAb (0.5 µg/ml) and anti-Tbr2 pAb (0.5 µg/ml). See Table S2 for full details of antibodies used. For histological analysis, paraffin sections were stained with Carazzi's Hematoxylin, Eosin Y and phloxine B (E6003 and P2759, Sigma-Aldrich). Slides for immunohistochemistry and histology were imaged under an upright microscope (DMR, Leica Microsystems) equipped with a CCD camera (Pro 600ES, Pixera).

Development (2022) 149, dev199931. doi:10.1242/dev.199931

X-gal staining

Embryos at E8.5 or E9.5 were fixed in 2% PFA/PBS at 4°C for 10 or 15 min, rinsed three times in 0.1 M phosphate buffer (pH 7.5) with 2 mM $MgCl_2$, 0.01% sodium deoxycholate and 0.02% NP-40, and then stained at 37°C overnight or for 1 h in the same detergent solution supplemented with 1 mg/ml X-gal (a stock solution at 25 mg/ml in N,N-dimethylformamide), 5 mM $K_3[Fe(CN)_6]$ and 5 mM $K_4[Fe(CN)_6]$. The stained embryos were post-fixed in 4% PFA/PBS(–) at room temperature for 3 h and photographed under a stereo microscope (MZ APO, Leica Microsystems) equipped with a CCD camera (Pro 600ES, Pixera).

Scanning electron microscopy

Dissected heads of embryos at E10.5 were mid-sagittally opened with a 76-µm-thick cutting blade (4761, Nisshin EM) to expose the telencephalic ventricle, gently flushed with PBS, fixed overnight at 4°C in 2.5% glutaraldehyde/0.1 M phosphate buffer (pH 7.4), and post-fixed in 1% OsO4/0.1 M phosphate buffer (pH 7.4). After dehydration through a graded ethanol series, samples were transferred to *t*-butyl alcohol, and freeze-dried with a freeze dryer (ES-2030, Hitachi High-Technologies). After mounting on aluminum stubs with carbon paste, the specimens were coated with osmium with an osmium plasma coater (OPC80T, Filgen), and observed using a field-emission scanning electron microscope (S-4800, Hitachi High-Technologies).

RNA extraction, reverse transcription and quantitative PCR (RT-qPCR)

The whole telencephalon or limb buds at E10.5 were dissected from each embryo in ice-cold PBS(–) under a stereo microscope (MZ APO, Leica Microsystems) and stored in RNAlater (AM7020, Ambion) at −20°C. Total RNA was extracted from each tissue and concentrated using QIAshredder (79656, QIAGEN), RNeasy Plus Mini Kit (74134, QIAGEN) and Agencourt RNAClean XP (A63987, Beckman Coulter). For RT-qPCR, total mRNA was reverse-transcribed using the High Capacity cDNA Reverse Transcription kit (4368814, Applied Biosystems). The threshold cycle (Ct) values were determined by RT-qPCR using qPCR Master Mix Plus (312-80291, Nippon Gene) and a MyiQ Single Color Real Time PCR Detection System (Bio-Rad) with TaqMan probes (Tables S3 and S4). The transcript levels were normalized to *18S* rRNA (*Rn18s*), and relative ratios to one of the control samples were calculated with the $2^{-\Delta\Delta Ct}$ method using iQ5 Optical System Software (v2.0, Bio-Rad; Table S4). Statistical analyses to compare each pair of results were performed using two-tailed Welch's *t*-test in R statistical software (Table S4). The results are presented using R statistical software as bee-swarm plots (Table S4) merged with box-whisker plots or bar graphs showing mean+s.d., if applicable.

Primary neurospheres

Primary neurospheres were prepared according to previous reports (Nagao et al., 2008; Reynolds and Weiss, 1996) with some modifications. The whole telencephalon at E11.5 was manually dissected in ice-cold artificial cerebrospinal fluid (10 mM HEPES-NaOH, pH 7.4, 124 mM NaCl, 5 mM KCl, 1 mM $MgCl_2$, 1 mM $CaCl_2$, 10 mM D-glucose) supplemented with 100 U/ml penicillin and 100 µg/ml streptomycin, incubated in dissociation solution (0.02% EDTA, 0.25% Trypsin, 1000 U/ml DNaseI, 1600 U/ml hyaluronidase type IV-S in PBS) at 37°C for 20 min, and then gently triturated in Neurobasal Medium (21103-049, Gibco) containing 1.0 mg/ml soybean trypsin inhibitor (109878, Roche). The residual meninges were removed, and the neural cells were resuspended in a media hormone mix [MHM; Neurobasal Medium containing 2% B27 supplement minus vitamin A (Gibco, 12587-010), 20 ng/ml EGF (AF-100-15, PeproTech), 20 ng/ml basic FGF (233-FB, R&D Systems), 0.5 mM L-glutamine, penicillin (100 U/ml) and streptomycin (100 µg/ml)]. After the dissociated cells were allowed to settle for 5 min, they were seeded onto two low-attachment dishes (9 cm^2 area; MS-9035X, Sumilon) containing MHM, and cultured for 3 days to form neurospheres. The neurospheres were divided into three 9-cm^2 low-attachment dishes, each containing MHM with 0, 15 or 40 nM SANT-1 (559303, EMD Millipore) along with 0.08% DMSO, cultured for 1 day, and then processed for RNA extraction.

Constructs

The SRD5/Ptch1-YFP/FRT-Hyg or SRD5/YFP-Smo/FRT-Hyg vectors were constructed from mouse Patched1 tagged with YFP at the C terminus (Rohatgi et al., 2007) or mouse smoothened tagged with YFP at the N terminus (Dorn et al., 2012) (pCS2+ YFP-Smo, Addgene plasmid #41086), in the SRD YK539 (Ohno et al., 1988), pcDNA5/FRT (V601020, Invitrogen) and pNL2.1[Nluc/Hygro] vectors (N1061, Promega) using PCR, a ligation kit (6022, Takara Bio) and a Gibson Assembly Kit (E2611, New England Biolabs Japan).

Stable cell lines

NIH 3T3 Flp-In cells (R761-07, lot 1146559, Life Technologies) stably expressing Ptch1-YFP or YFP-Smo were respectively established by co-transfection of pCAGGS-Flpo-IRES-Puro (Kranz et al., 2010) with SRD5/Ptch1-YFP/FRT-Hyg (1:3) or SRD5/YFP-Smo/FRT-Hyg (1:1) using PolyFect (301107, lot 136246701, QIAGEN), following selection with hygromycin B (089-06151, Wako Pure Chemicals) at 200 µg/ml for 15 or 12 days. The isolated colonies were expanded, and then confirmed by immunoblotting and immunofluorescence. The established cell lines (clone 3B, Flp-In-3T3/Ptch1-YFP; clone F3, Flp-In-3T3/YFP-Smo) were grown in Dulbecco's modified Eagle's medium (05919, Nissui Pharmaceutical) supplemented with 7% calf serum (16170-078, Gibco), 4 mM L-glutamine, 100 U/ml penicillin, 100 µg/ml streptomycin and 0.15% sodium bicarbonate. siRNA-mediated gene silencing was performed for two consecutive days using siLentFect (1703362, Bio-Rad) with 20 nM of each siRNA listed in Table S3.

Quantification and statistical analysis

The distances of CldU- or IdU-labeled nuclei, or mitotic nuclei from the ventricular surface were analyzed using ImageJ (Schneider et al., 2012) (NIH). The angles of the cleavage plane orientation for mitotic NPCs, and the immunoblotting results were analyzed using Multi Gauge software (v2.2, Fujifilm). The numbers of analyzed embryos and cells are indicated in the figure legends. Statistical analyses to compare each pair of results were performed using the Brunner–Munzel test (Brunner and Munzel, 2000; Neubert and Brunner, 2007) using R statistical software (Table S4).

To measure the ciliary length in the telencephalon, deconvoluted finite super-resolution images were reconstructed into maximal intensity projection images, and Arl13b-positive regions were measured using ImageJ. The intensities of YFP-tagged proteins or acetylated α-tubulin in fibroblasts were measured in epifluorescence microscope images using ImageJ, and intensities of YFP-tagged proteins were normalized against acetylated α-tubulin. To measure the ciliary intensities of Smo and IFT88 in the telencephalon, ciliary regions were quantified along with *z*-slices of deconvoluted finite super-resolution images using ImageJ. The results are presented using R statistical software as bee-swarm plots merged with box-whisker plots or violin plots (Table S4). The numbers of cilia and embryos analyzed are indicated in the figure legends. The Brunner–Munzel test was performed using R statistical software with the brunnermunzel package by Toshiaki Ara (Table S4).

Acknowledgements

We thank J. M. Hébert and S. K. McConnell for providing *Foxg1-Cre* mice; T. Yagi, R. Rohatgi, M. P. Scott, F. Stewart and A. Yamashita for sharing the expression vectors; H. Yamanaka, S. Ito, M. Fukuda, A. Kawaguchi and M. Tanaka for assistance in establishing and maintaining mouse lines; J. Nakamoto for supporting sample preparation and observation of scanning electron microscopy; S. Goulas for valuable suggestions and encouragement; and all the members of the Noda, Takahashi and Ohno laboratories for stimulating discussions and helpful comments. Mice were maintained in the animal facilities of Yokohama City University School of Medicine and the Cancer Institute of the Japanese Foundation for Cancer Research. Part of this work was carried out at the Research Support Center of Juntendo University. We thank Barry Patel, PhD, and J. Ludovic Croxford, PhD, from Edanz for editing a draft of the manuscript.

Competing interests

The authors declare no competing or financial interests.

Author contributions

Conceptualization: T.H.; Methodology: T.H., Y.S., H. Kurihara, H. Kazama, C.K., T.N.; Formal analysis: T.H.; Investigation: T.H., H. Kurihara, H. Kazama, C.K.;

Writing - original draft: T.H.; Writing - review & editing: T.H., Y.S., H.T., S.O.; Supervision: S.O.; Project administration: T.H., T.N., S.O.; Funding acquisition: T.H., T.N., H.T., S.O.

Funding

This work was supported by a Grant-in-Aid for Scientific Research on Innovative Areas 'Neural Diversity and Neocortical Organization' from the Ministry of Education, Culture, Sports, Science and Technology (MEXT) of Japan (JP23123518 to T.H.), Japan Society for the Promotion of Science KAKENHI (JP23790342 and JP20K06893 to T.H.), and the Yokohama Foundation for Advanced Medical Science (T.H.); in part by a Grant-in-Aid for Scientific Research on Innovative Areas 'Tubulology' from MEXT (to S.O.) and a grant for the Creation of Innovation Centers for Advanced Interdisciplinary Research Areas Program from MEXT (to S.O.); and in part by grants from the MSD Life Science Foundation, Public Interest Incorporated Foundation, the Naito Foundation, and the Uehara Memorial Foundation (H.T.).

Peer review history

The peer review history is available online at https://journals.biologists.com/dev/lookup/doi/10.1242/dev.199931.reviewer-comments.pdf.

References

Atwood, S. X., Li, M., Lee, A., Tang, J. Y. and Oro, A. E. (2013). GLI activation by atypical protein kinase C ι/λ regulates the growth of basal cell carcinomas. *Nature* **494**, 484-488. doi:10.1038/nature11889

Bangs, F. and Anderson, K. V. (2017). Primary cilia and mammalian hedgehog signaling. *Cold Spring Harb. Perspect. Biol.* **9**, a028175. doi:10.1101/cshperspect.a028175

Borlinghaus, R. T. and Kappel, C. (2016). HyVolution – the smart path to confocal super-resolution. *Nat. Methods* **13**, i-iii. doi:10.1038/nmeth.f.392

Briscoe, J. and Thérond, P. P. (2013). The mechanisms of Hedgehog signalling and its roles in development and disease. *Nat. Rev. Mol. Cell Biol.* **14**, 416-429. doi:10.1038/nrm3598

Brunner, E. and Munzel, U. (2000). The nonparametric Behrens-Fisher problem: asymptotic theory and a small-sample approximation. *Biom. J.* **42**, 17-25. doi:10.1002/(SICI)1521-4036(200001)42:1<17::AID-BIMJ17>3.0.CO;2-U

Bultje, R. S., Castaneda-Castellanos, D. R., Jan, L. Y., Jan, Y.-N., Kriegstein, A. R. and Shi, S.-H. (2009). Mammalian Par3 regulates progenitor cell asymmetric division via notch signaling in the developing neocortex. *Neuron* **63**, 189-202. doi:10.1016/j.neuron.2009.07.004

Calegari, F. (2005). Selective lengthening of the cell cycle in the neurogenic subpopulation of neural progenitor cells during mouse brain development. *J. Neurosci.* **25**, 6533-6538. doi:10.1523/JNEUROSCI.0778-05.2005

Cappello, S., Attardo, A., Wu, X., Iwasato, T., Itohara, S., Wilsch-Bräuninger, M., Eilken, H. M., Rieger, M. A., Schroeder, T. T., Huttner, W. B. et al. (2006). The Rho-GTPase cdc42 regulates neural progenitor fate at the apical surface. *Nat. Neurosci.* **9**, 1099-1107. doi:10.1038/nn1744

Chen, J. K., Taipale, J., Young, K. E., Maiti, T. and Beachy, P. A. (2002). Small molecule modulation of Smoothened activity. *Proc. Natl. Acad. Sci. USA* **99**, 14071-14076. doi:10.1073/pnas.182542899

Corbit, K. C., Aanstad, P., Singla, V., Norman, A. R., Stainier, D. Y. R. and Reiter, J. F. (2005). Vertebrate Smoothened functions at the primary cilium. *Nature* **437**, 1018-1021. doi:10.1038/nature04117

Costa, M. R., Wen, G., Lepier, A., Schroeder, T. and Götz, M. (2008). Par-complex proteins promote proliferative progenitor divisions in the developing mouse cerebral cortex. *Development* **135**, 11-22. doi:10.1242/dev.009951

Dorn, K. V., Hughes, C. E. and Rohatgi, R. (2012). A smoothened-Evc2 complex transduces the hedgehog signal at primary cilia. *Dev. Cell* **23**, 823-835. doi:10.1016/j.devcel.2012.07.004

Englund, C. (2005). Pax6, Tbr2, and Tbr1 are expressed sequentially by radial glia, intermediate progenitor cells, and postmitotic neurons in developing neocortex. *J. Neurosci.* **25**, 247-251. doi:10.1523/JNEUROSCI.2899-04.2005

Fietz, S. A., Kelava, I., Vogt, J., Wilsch-Bräuninger, M., Stenzel, D., Fish, J. L., Corbeil, D., Riehn, A., Distler, W., Nitsch, R. et al. (2010). OSVZ progenitors of human and ferret neocortex are epithelial-like and expand by integrin signaling. *Nat. Neurosci.* **13**, 690-699. doi:10.1038/nn.2553

Fish, J. L., Kosodo, Y., Enard, W., Paabo, S. and Huttner, W. B. (2006). Aspm specifically maintains symmetric proliferative divisions of neuroepithelial cells. *Proc. Natl. Acad. Sci. USA* **103**, 10438-10443. doi:10.1073/pnas.0604066103

Fuccillo, M., Rallu, M., Mcmahon, A. P. and Fishell, G. (2004). Temporal requirement for hedgehog signaling in ventral telencephalic patterning. *Development* **131**, 5031-5040. doi:10.1242/dev.01349

Fujita, I., Shitamukai, A., Kusumoto, F., Mase, S., Suetsugu, T., Omori, A., Kato, K., Abe, T., Shioi, G., Konno, D. et al. (2020). Endfoot regeneration restricts radial glial state and prevents translocation into the outer subventricular zone in early mammalian brain development. *Nat. Cell Biol.* **22**, 26-37. doi:10.1038/s41556-019-0436-9

Goetz, S. C. and Anderson, K. V. (2010). The primary cilium: a signalling centre during vertebrate development. *Nat. Rev. Genet.* **11**, 331-344. doi:10.1038/nrg2774

Guemez-Gamboa, A., Coufal, N. G. and Gleeson, J. G. (2014). Primary cilia in the developing and mature brain. *Neuron* **82**, 511-521. doi:10.1016/j.neuron.2014.04.024

Guillemot, F. and Joyner, A. L. (1993). Dynamic expression of the murine Achaete-Scute homologue Mash-1 in the developing nervous system. *Mech. Dev.* **42**, 171-185. doi:10.1016/0925-4773(93)90006-J

Hansen, D. V., Lui, J. H., Parker, P. R. L. and Kriegstein, A. R. (2010). Neurogenic radial glia in the outer subventricular zone of human neocortex. *Nature* **464**, 554-561. doi:10.1038/nature08845

Hatakeyama, J., Bessho, Y., Katoh, K., Ookawara, S., Fujioka, M., Guillemot, F. and Kageyama, R. (2004). Hes genes regulate size, shape and histogenesis of the nervous system by control of the timing of neural stem cell differentiation. *Development* **131**, 5539-5550. doi:10.1242/dev.01436

Haubensak, W., Attardo, A., Denk, W. and Huttner, W. B. (2004). Neurons arise in the basal neuroepithelium of the early mammalian telencephalon: a major site of neurogenesis. *Proc. Natl. Acad. Sci. USA* **101**, 3196-3201. doi:10.1073/pnas.0308600100

Haycraft, C. J., Banizs, B., Aydin-Son, Y., Zhang, Q., Michaud, E. J. and Yoder, B. K. (2005). Gli2 and Gli3 localize to cilia and require the intraflagellar transport protein polaris for processing and function. *PLoS Genet.* **1**, e53. doi:10.1371/journal.pgen.0010053

Hébert, J. M. and Mcconnell, S. K. (2000). Targeting of cre to the Foxg1 (BF-1) locus mediates loxP recombination in the telencephalon and other developing head structures. *Dev. Biol.* **222**, 296-306. doi:10.1006/dbio.2000.9732

Higginbotham, H., Guo, J., Yokota, Y., Umberger, N. L., Su, C. Y., Li, J., Verma, N., Hirt, J., Ghukasyan, V., Caspary, T. et al. (2013). Arl13b-regulated cilia activities are essential for polarized radial glial scaffold formation. *Nat. Neurosci.* **16**, 1000-1007. doi:10.1038/nn.3451

Hirabayashi, Y., Itoh, Y., Tabata, H., Nakajima, K., Akiyama, T., Masuyama, N. and Gotoh, Y. (2004). The Wnt/beta-catenin pathway directs neuronal differentiation of cortical neural precursor cells. *Development* **131**, 2791-2801. doi:10.1242/dev.01165

Hirose, T., Karasawa, M., Sugitani, Y., Fujisawa, M., Akimoto, K., Ohno, S. and Noda, T. (2006). PAR3 is essential for cyst-mediated epicardial development by establishing apical cortical domains. *Development* **133**, 1389-1398. doi:10.1242/dev.02294

Horikoshi, Y., Suzuki, A., Yamanaka, T., Sasaki, K., Mizuno, K., Sawada, H., Yonemura, S. and Ohno, S. (2009). Interaction between PAR-3 and the aPKC-PAR-6 complex is indispensable for apical domain development of epithelial cells. *J. Cell Sci.* **122**, 1595-1606. doi:10.1242/jcs.043174

Iden, S., Van Riel, W. E., Schafer, R., Song, J. Y., Hirose, T., Ohno, S. and Collard, J. G. (2012). Tumor type-dependent function of the par3 polarity protein in skin tumorigenesis. *Cancer Cell* **22**, 389-403. doi:10.1016/j.ccr.2012.08.004

Imai, F., Hirai, S., Akimoto, K., Koyama, H., Miyata, T., Ogawa, M., Noguchi, S., Sasaoka, T., Noda, T. and Ohno, S. (2006). Inactivation of aPKCλ results in the loss of adherens junctions in neuroepithelial cells without affecting neurogenesis in mouse neocortex. *Development* **133**, 1735-1744. doi:10.1242/dev.02330

Incardona, J. P., Gaffield, W., Kapur, R. P. and Roelink, H. (1998). The teratogenic Veratrum alkaloid cyclopamine inhibits Sonic hedgehog signal transduction. *Development* **125**, 3553-3562. doi:10.1242/dev.125.18.3553

Jossin, Y., Lee, M., Klezovitch, O., Kon, E., Cossard, A., Lien, W.-H., Fernandez, T. E., Cooper, J. A. and Vasioukhin, V. (2017). Llgl1 Connects Cell Polarity with Cell-Cell Adhesion in Embryonic Neural Stem Cells. *Dev. Cell* **41**, 481-495.e5. doi:10.1016/j.devcel.2017.05.002

Kawaguchi, A., Ikawa, T., Kasukawa, T., Ueda, H. R., Kurimoto, K., Saitou, M. and Matsuzaki, F. (2008). Single-cell gene profiling defines differential progenitor subclasses in mammalian neurogenesis. *Development* **135**, 3113-3124. doi:10.1242/dev.022616

Komada, M., Saitsu, H., Kinboshi, M., Miura, T., Shiota, K. and Ishibashi, M. (2008). Hedgehog signaling is involved in development of the neocortex. *Development* **135**, 2717-2727. doi:10.1242/dev.015891

Kovacs, J. J., Whalen, E. J., Liu, R., Xiao, K., Kim, J., Chen, M., Wang, J., Chen, W. and Lefkowitz, R. J. (2008). Beta-arrestin-mediated localization of smoothened to the primary cilium. *Science* **320**, 1777-1781. doi:10.1126/science.1157983

Kranz, A., Fu, J., Duerschke, K., Weidlich, S., Naumann, R., Stewart, A. F. and Anastassiadis, K. (2010). An improved Flp deleter mouse in C57Bl/6 based on Flpo recombinase. *Genesis* **48**, 512-520. doi:10.1002/dvg.20641

Lamonica, B. E., Lui, J. H., Wang, X. and Kriegstein, A. R. (2012). OSVZ progenitors in the human cortex: an updated perspective on neurodevelopmental disease. *Curr. Opin. Neurobiol.* **22**, 747-753. doi:10.1016/j.conb.2012.03.006

Liu, W. A., Chen, S., Li, Z., Lee, C. H., Mirzaa, G., Dobyns, W. B., Ross, M. E., Zhang, J. and Shi, S.-H. (2018). PARD3 dysfunction in conjunction with dynamic HIPPO signaling drives cortical enlargement with massive heterotopia. *Genes Dev.* **32**, 763-780. doi:10.1101/gad.313171.118

Liu, S., Trupiano, M. X., Simon, J., Guo, J. and Anton, E. S. (2021). The essential role of primary cilia in cerebral cortical development and disorders. *Curr. Top. Dev. Biol.* **142**, 99-146. doi:10.1016/bs.ctdb.2020.11.003

Lui, J. H., Hansen, D. V. and Kriegstein, A. R. (2011). Development and evolution of the human neocortex. *Cell* **146**, 18-36. doi:10.1016/j.cell.2011.06.030

Manabe, N., Hirai, S.-I., Imai, F., Nakanishi, H., Takai, Y. and Ohno, S. (2002). Association of ASIP/mPAR-3 with adherens junctions of mouse neuroepithelial cells. *Dev. Dyn.* **225**, 61-69. doi:10.1002/dvdy.10139

Martínez-Martínez, M. Á., De Juan Romero, C., Fernández, V., Cárdenas, A., Götz, M. and Borrell, V. (2016). A restricted period for formation of outer subventricular zone defined by Cdh1 and Trnp1 levels. *Nat. Commun.* **7**, 11812. doi:10.1038/ncomms11812

Matsumoto, N., Tanaka, S., Horiike, T., Shinmyo, Y. and Kawasaki, H. (2020). A discrete subtype of neural progenitor crucial for cortical folding in the gyrencephalic mammalian brain. *Elife* **9**, e54873. doi:10.7554/eLife.54873

Matsuzaki, F. and Shitamukai, A. (2015). Cell division modes and cleavage planes of neural progenitors during mammalian cortical development. *Cold Spring Harb. Perspect. Biol.* **7**, a015719. doi:10.1101/cshperspect.a015719

Mccaffrey, L. M. and Macara, I. G. (2009). The Par3/aPKC interaction is essential for end bud remodeling and progenitor differentiation during mammary gland morphogenesis. *Genes Dev.* **23**, 1450-1460. doi:10.1101/gad.1795909

Mclean, I. W. and Nakane, P. K. (1974). Periodate-lysine-paraformaldehyde fixative. A new fixation for immunoelectron microscopy. *J. Histochem. Cytochem.* **22**, 1077-1083. doi:10.1177/22.12.1077

Milenkovic, L., Scott, M. P. and Rohatgi, R. (2009). Lateral transport of smoothened from the plasma membrane to the membrane of the cilium. *J. Cell Biol.* **187**, 365-374. doi:10.1083/jcb.200907126

Miyata, T., Kawaguchi, A., Saito, K., Kawano, M., Muto, T. and Ogawa, M. (2004). Asymmetric production of surface-dividing and non-surface-dividing cortical progenitor cells. *Development* **131**, 3133-3145. doi:10.1242/dev.01173

Miyata, T., Kawaguchi, D., Kawaguchi, A. and Gotoh, Y. (2010). Mechanisms that regulate the number of neurons during mouse neocortical development. *Curr. Opin. Neurobiol.* **20**, 22-28. doi:10.1016/j.conb.2010.01.001

Mizutani, K., Yoon, K., Dang, L., Tokunaga, A. and Gaiano, N. (2007). Differential Notch signalling distinguishes neural stem cells from intermediate progenitors. *Nature* **449**, 351-355. doi:10.1038/nature06090

Muzio, L. and Mallamaci, A. (2005). Foxg1 confines Cajal-Retzius neuronogenesis and hippocampal morphogenesis to the dorsomedial pallium. *J. Neurosci.* **25**, 4435-4441. doi:10.1523/JNEUROSCI.4804-04.2005

Nagao, M., Campbell, K., Burns, K., Kuan, C.-Y., Trumpp, A. and Nakafuku, M. (2008). Coordinated control of self-renewal and differentiation of neural stem cells by Myc and the p19ARF–p53 pathway. *J. Cell Biol.* **183**, 1243-1257. doi:10.1083/jcb.200807130

Neubert, K. and Brunner, E. (2007). A studentized permutation test for the non-parametric Behrens–Fisher problem. *Comput. Stat. Data Anal.* **51**, 5192-5204. doi:10.1016/j.csda.2006.05.024

Noctor, S. C., Flint, A. C., Weissman, T. A., Dammerman, R. S. and Kriegstein, A. R. (2001). Neurons derived from radial glial cells establish radial units in neocortex. *Nature* **409**, 714-720. doi:10.1038/35055553

Noctor, S. C., Martínez-Cerdeño, V., Ivic, L. and Kriegstein, A. R. (2004). Cortical neurons arise in symmetric and asymmetric division zones and migrate through specific phases. *Nat. Neurosci.* **7**, 136-144. doi:10.1038/nn1172

Ohno, S., Akita, Y., Konno, Y., Imajoh, S. and Suzuki, K. (1988). A novel phorbol ester receptor/protein kinase, nPKC, distantly related to the protein kinase C family. *Cell* **53**, 731-741. doi:10.1016/0092-8674(88)90091-8

Ohno, S., Goulas, S. and Hirose, T. (2015). The PAR3-aPKC-PAR6 complex. In *Cell Polarity 1* (ed. K. Ebnet), pp. 3-23. Cham, Switzerland: Springer International Publishing.

Palma, V. and Ruiz i Altaba, A. (2004). Hedgehog-GLI signaling regulates the behavior of cells with stem cell properties in the developing neocortex. *Development* **131**, 337-345. doi:10.1242/dev.00930

Pazour, G. J., Baker, S. A., Deane, J. A., Cole, D. G., Dickert, B. L., Rosenbaum, J. L., Witman, G. B. and Besharse, J. C. (2002). The intraflagellar transport protein, IFT88, is essential for vertebrate photoreceptor assembly and maintenance. *J. Cell Biol.* **157**, 103-114. doi:10.1083/jcb.200107108

Postiglione, M. P., Jüschke, C., Xie, Y., Haas, G. A., Charalambous, C. and Knoblich, J. A. (2011). Mouse inscuteable induces apical-basal spindle orientation to facilitate intermediate progenitor generation in the developing neocortex. *Neuron* **72**, 269-284. doi:10.1016/j.neuron.2011.09.022

Rakic, P. (1995). A small step for the cell, a giant leap for mankind: a hypothesis of neocortical expansion during evolution. *Trends Neurosci.* **18**, 383-388. doi:10.1016/0166-2236(95)93934-P

Rallu, M., Machold, R., Gaiano, N., Corbin, J. G., Mcmahon, A. P. and Fishell, G. (2002). Dorsoventral patterning is established in the telencephalon of mutants lacking both Gli3 and Hedgehog signaling. *Development* **129**, 4963-4974. doi:10.1242/dev.129.21.4963

Reynolds, B. A. and Weiss, S. (1996). Clonal and population analyses demonstrate that an EGF-responsive mammalian embryonic CNS precursor is a stem cell. *Dev. Biol.* **175**, 1-13. doi:10.1006/dbio.1996.0090

Rohatgi, R., Milenkovic, L. and Scott, M. P. (2007). Patched1 regulates hedgehog signaling at the primary cilium. *Science* **317**, 372-376. doi:10.1126/science.1139740

Sahara, S. and O'Leary, D. D. M. (2009). Fgf10 regulates transition period of cortical stem cell differentiation to radial glia controlling generation of neurons and basal progenitors. *Neuron* **63**, 48-62. doi:10.1016/j.neuron.2009.06.006

Sauer, F. C. (1935). Mitosis in the neural tube. *J. Comp. Neurol.* **62**, 377-405. doi:10.1002/cne.900620207

Schneider, L., Clement, C. A., Teilmann, S. C., Pazour, G. J., Hoffmann, E. K., Satir, P. and Christensen, S. T. (2005). PDGFRαα signaling is regulated through the primary cilium in fibroblasts. *Curr. Biol.* **15**, 1861-1866. doi:10.1016/j.cub.2005.09.012

Schneider, C. A., Rasband, W. S. and Eliceiri, K. W. (2012). NIH image to ImageJ: 25 years of image analysis. *Nat. Methods* **9**, 671-675. doi:10.1038/nmeth.2089

Sfakianos, J., Togawa, A., Maday, S., Hull, M., Pypaert, M., Cantley, L., Toomre, D. and Mellman, I. (2007). Par3 functions in the biogenesis of the primary cilium in polarized epithelial cells. *J. Cell Biol.* **179**, 1133-1140. doi:10.1083/jcb.200709111

Shen, L., Nam, H.-S., Song, P., Moore, H. and Anderson, S. A. (2006). FoxG1 haploinsufficiency results in impaired neurogenesis in the postnatal hippocampus and contextual memory deficits. *Hippocampus* **16**, 875-890. doi:10.1002/hipo.20218

Shimojo, H., Ohtsuka, T. and Kageyama, R. (2008). Oscillations in Notch signaling regulate maintenance of neural progenitors. *Neuron* **58**, 52-64. doi:10.1016/j.neuron.2008.02.014

Shitamukai, A., Konno, D. and Matsuzaki, F. (2011). Oblique radial glial divisions in the developing mouse neocortex induce self-renewing progenitors outside the germinal zone that resemble primate outer subventricular zone progenitors. *J. Neurosci.* **31**, 3683-3695. doi:10.1523/JNEUROSCI.4773-10.2011

Siegenthaler, J. A., Ashique, A. M., Zarbalis, K., Patterson, K. P., Hecht, J. H., Kane, M. A., Folias, A. E., Choe, Y., May, S. R., Kume, T. et al. (2009). Retinoic acid from the meninges regulates cortical neuron generation. *Cell* **139**, 597-609. doi:10.1016/j.cell.2009.10.004

Snedeker, J., Schock, E. N., Struve, J. N., Chang, C., Cionni, M., Tran, P. V., Brugmann, S. A. and Stottmann, R. W. (2017). Unique spatiotemporal requirements for intraflagellar transport genes during forebrain development. *PLoS One* **12**, e0173258. doi:10.1371/journal.pone.0173258

Soriano, P. (1999). Generalized lacZ expression with the ROSA26 Cre reporter strain. *Nat. Genet.* **21**, 70-71. doi:10.1038/5007

Sousa, V. H. and Fishell, G. (2010). Sonic hedgehog functions through dynamic changes in temporal competence in the developing forebrain. *Curr. Opin. Genet. Dev.* **20**, 391-399. doi:10.1016/j.gde.2010.04.008

Stoykova, A., Treichel, D., Hallonet, M. and Gruss, P. (2000). Pax6 modulates the dorsoventral patterning of the mammalian telencephalon. *J. Neurosci.* **20**, 8042-8050. doi:10.1523/JNEUROSCI.20-21-08042.2000

Takahashi, T., Nowakowski, R. S. and Caviness, V. (1995). The cell cycle of the pseudostratified ventricular epithelium of the embryonic murine cerebral wall. *J. Neurosci.* **15**, 6046-6057. doi:10.1523/JNEUROSCI.15-09-06046.1995

Takahashi, T., Nowakowski, R. S. and Caviness, V. S.Jr. (1996). Interkinetic and migratory behavior of a cohort of neocortical neurons arising in the early embryonic murine cerebral wall. *J. Neurosci.* **16**, 5762-5776. doi:10.1523/JNEUROSCI.16-18-05762.1996

Taniguchi, M., Sanbo, M., Watanabe, S., Naruse, I., Mishina, M. and Yagi, T. (1998). Efficient production of Cre-mediated site-directed recombinants through the utilization of the puromycin resistance gene, pac: a transient gene-integration marker for ES cells. *Nucleic Acids Res.* **26**, 679-680. doi:10.1093/nar/26.2.679

Takahashi, T., Goto, T., Miyama, S., Nowakowski, R. S. and Caviness, V. S. (1999). Sequence of neuron origin and neocortical laminar fate: relation to cell cycle of origin in the developing murine cerebral wall. *J. Neurosci.* **19**, 10357-10371. doi:10.1523/JNEUROSCI.19-23-10357.1999

Taverna, E., Götz, M. and Huttner, W. B. (2014). The cell biology of neurogenesis: toward an understanding of the development and evolution of the neocortex. *Annu. Rev. Cell Dev. Biol.* **30**, 465-502. doi:10.1146/annurev-cellbio-101011-155801

Taylor, F. R., Wen, D., Garber, E. A., Carmillo, A. N., Baker, D. P., Arduini, R. M., Williams, K. P., Weinreb, P. H., Rayhorn, P., Hronowski, X. et al. (2001). Enhanced potency of human sonic hedgehog by hydrophobic modification. *Biochemistry* **40**, 4359-4371. doi:10.1021/bi002487u

Tong, C. K., Han, Y.-G., Shah, J. K., Obernier, K., Guinto, C. D. and Alvarez-Buylla, A. (2014). Primary cilia are required in a unique subpopulation of neural progenitors. *Proc. Natl. Acad. Sci. USA* **111**, 12438-12443. doi:10.1073/pnas.1321425111

Toresson, H., Potter, S. S. and Campbell, K. (2000). Genetic control of dorsal-ventral identity in the telencephalon: opposing roles for Pax6 and Gsh2. *Development* **127**, 4361-4371. doi:10.1242/dev.127.20.4361

Vokes, S. A., Ji, H., Mccuine, S., Tenzen, T., Giles, S., Zhong, S., Longabaugh, W. J. R., Davidson, E. H., Wong, W. H. and Mcmahon, A. P. (2007). Genomic characterization of Gli-activator targets in sonic hedgehog-mediated neural patterning. *Development* **134**, 1977-1989. doi:10.1242/dev.001966

Wang, L., Hou, S. and Han, Y.-G. (2016). Hedgehog signaling promotes basal progenitor expansion and the growth and folding of the neocortex. *Nat. Neurosci.* **19**, 888-896. doi:10.1038/nn.4307

Wang, B., Fallon, J. F. and Beachy, P. A. (2000). Hedgehog-regulated processing of Gli3 produces an anterior/posterior repressor gradient in the developing vertebrate limb. *Cell* **100**, 423-434. doi:10.1016/S0092-8674(00)80678-9

Willaredt, M. A., Tasouri, E. and Tucker, K. L. (2013). Primary cilia and forebrain development. *Mech. Dev.* **130**, 373-380. doi:10.1016/j.mod.2012.10.003

Wilson, S. L., Wilson, J. P., Wang, C., Wang, B. and Mcconnell, S. K. (2012). Primary cilia and Gli3 activity regulate cerebral cortical size. *Dev. Neurobiol.* **72**, 1196-1212. doi:10.1002/dneu.20985

Woodhead, G. J., Mutch, C. A., Olson, E. C. and Chenn, A. (2006). Cell-autonomous beta-catenin signaling regulates cortical precursor proliferation. *J. Neurosci.* **26**, 12620-12630. doi:10.1523/JNEUROSCI.3180-06.2006

Yabut, O. R. and Pleasure, S. J. (2018). Sonic Hedgehog signaling rises to the surface: emerging roles in neocortical development. *Brain Plast.* **3**, 119-128. doi:10.3233/BPL-180064

Yingling, J., Youn, Y. H., Darling, D., Toyo-Oka, K., Pramparo, T., Hirotsune, S. and Wynshaw-Boris, A. (2008). Neuroepithelial stem cell proliferation requires LIS1 for precise spindle orientation and symmetric division. *Cell* **132**, 474-486. doi:10.1016/j.cell.2008.01.026

Zimmerman, L., Parr, B., Lendahl, U., Cunningham, M., Mckay, R., Gavin, B., Mann, J., Vassileva, G. and Mcmahon, A. (1994). Independent regulatory elements in the nestin gene direct transgene expression to neural stem cells or muscle precursors. *Neuron* **12**, 11-24. doi:10.1016/0896-6273(94)90148-1